Energy Reports 15 (2026) 109327

Contents lists available at ScienceDirect

Energy Reports

journal homepage: www.elsevier.com/locate/egyr

Research paper

Techno-economic analysis of Ocean Thermal Energy Conversion (OTEC): The influence of cold seawater depth

Ristiyanto Adiputra [a], Dani Irianto [b], Zakie Anugia [b], Donny Mustika [b], Kartika Raras Hadiyati [b], Fauzan Adhi Sasmita [b], Muhammad Suistama Sofan Hadi [b], Arrester Christiana Slamet Rahayu [b], Dwi Rian Sulaeman [b], Mukhtasor [c,*]

[a] Research Center for Hydrodynamics Technology, National Research and Innovation Agency (BRIN), Tangerang Selatan 15310, Indonesia
[b] PT Perusahaan Listrik Negara (Persero), Jakarta 12160, Indonesia
[c] Department of Ocean Engineering, Faculty of Marine Technology, Institut Teknologi Sepuluh Nopember, Surabaya 60111, Indonesia

ARTICLE INFO

Keywords:
OTEC
Efficiency
LCOE
Temperature differences
Single-stage rankine cycle

ABSTRACT

Ocean Thermal Energy Conversion (OTEC) is a promising renewable energy technology that utilizes the temperature difference between surface and deep seawater to generate electricity. However, its implementation faces significant challenges, particularly related to the design and cost of cold seawater intake infrastructure. This study investigates the influence of deep seawater intake depth (350, 400, 500, 600, and 700 m) on the technical performance and economic feasibility of an OTEC system using Manado Bay, Indonesia, as a case study. Temperature profiles derived from HYCOM data were combined with a single-stage Rankine cycle model to evaluate system efficiency, component sizing, and the Levelized Cost of Electricity (LCOE). The thermodynamic model was validated against experimental results reported in the literature, showing good agreement and confirming the reliability of the adopted approach. The results indicate that increasing the intake depth enhances the thermal gradient, which improves system performance and reduces the required mass flow rates of seawater and working fluid. Consequently, the heat exchanger area and associated capital costs decrease with increasing depth. The system operating with a 700 m intake depth achieved the highest thermal efficiency of 3.75% and the lowest LCOE of 8.31 USD cents/kWh. Sensitivity analysis further shows that LCOE is strongly affected by variations in CAPEX and OPEX, particularly those associated with platform and heat exchanger costs. These findings provide useful insights for optimizing OTEC system design and improving the economic feasibility of renewable energy deployment in tropical coastal regions.

1. Introduction

The ocean is one of the most abundant sources of renewable energy, and Ocean Thermal Energy Conversion (OTEC) represents a promising technology to harness this resource (Faizatama et al., 2025). The basic principle of a closed-cycle OTEC system is based on the Rankine cycle (see Fig. 1), where warm surface seawater vaporizes a low-boiling-point working fluid, which expands through a turbine to generate electricity (Habib et al., 2023; Rasgianti et al., 2024c). The vapor is subsequently condensed using cold deep seawater, completing the thermodynamic cycle. Due to the relatively stable thermal gradient in tropical regions, OTEC systems are capable of continuous power generation and can serve as a reliable baseload energy source (Adiputra et al., 2025; Adiputra and Utsunomiya, 2021). Nevertheless, system performance and economic feasibility are strongly influenced by environmental conditions, component design, and especially the depth of cold seawater intake.

Extensive studies have focused on improving the thermodynamic performance of OTEC systems by enhancing heat transfer and cycle efficiency. It has been demonstrated that increasing warm seawater temperature and reducing cold seawater temperature significantly improve turbine inlet conditions, net power output, and overall efficiency (Kim et al., 2016; Mao et al., 2023; Yang and Yeh, 2014). Heat exchanger design optimization, including geometric refinement and surface enhancement, has been shown to increase net power density while reducing entropy generation (Fontaine et al., 2025). Solar-assisted OTEC concepts have been proposed to elevate the temperature of the warm seawater inlet, thereby enhancing system efficiency and energy output under certain climatic conditions (Prasad et al., 2025; Rami and Allouhi,

* Corresponding author.
E-mail address: mukhtasor@oe.its.ac.id (Mukhtasor).

https://doi.org/10.1016/j.egyr.2026.109327
Received 4 August 2025; Received in revised form 8 March 2026; Accepted 11 April 2026
Available online 16 April 2026

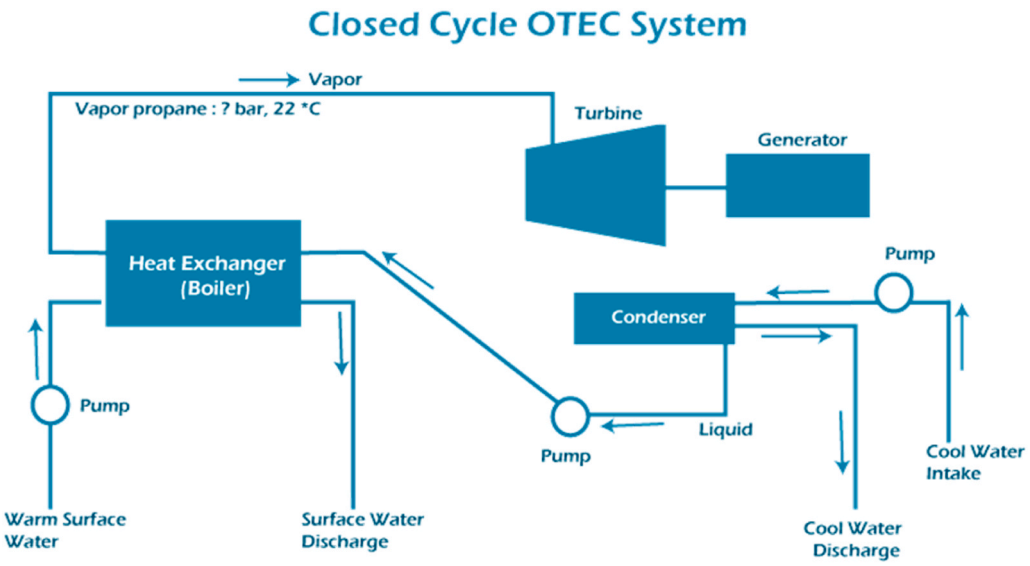

Fig. 1. Closed Cycle OTEC System.

2024; Wang et al., 2024). Additionally, pressure energy recovery systems and alternative thermodynamic configurations have been proposed to enhance overall system efficiency (Tian et al., 2024). These studies collectively confirm that thermal gradient management and heat exchanger performance are central to OTEC efficiency improvement.

Another major line of research concerns working fluid selection and advanced system optimization. The choice of working fluid significantly affects evaporation and condensation characteristics, turbine work, and pumping requirements. Investigations into pure and mixed working fluids, as well as fluid charging conditions, have demonstrated substantial impacts on thermal and exergy efficiency (Achkienasi et al., 2024; Zhang et al., 2024; Zhou et al., 2025). In addition, recent studies have increasingly integrated thermodynamic, economic, and exergoeconomic perspectives to evaluate system feasibility and cost distribution across components.

Several recent works have focused on parameter sensitivity and system performance under tropical ocean conditions. (Puryantini et al., 2026) analyzed the influence of key efficiency parameters on the net power output of a 10 MW ORC-based OTEC system using Aspen Plus. Their results showed that turbine efficiency is the dominant factor affecting net power, followed by seawater pump efficiency, while variations in seawater temperature had a limited effect when flow rates were kept constant. Similarly, (Rasgianti et al., 2024b) conducted sensitivity analysis under Indonesian ocean conditions and confirmed the strong dependence of net power output and system efficiency on thermal gradients and heat exchanger configuration. These findings highlight the importance of component-level optimization in addition to site-specific thermal assessment.

Working fluid selection has also been examined through comprehensive evaluation frameworks that consider not only thermodynamic performance but also safety, environmental impact, and equipment implications. (Adiputra et al., 2025) performed a multi-stage assessment of candidate working fluids and identified ammonia as the most suitable option for OTEC systems. This result reinforces the importance of integrated performance evaluation, as working fluid choice directly influences cycle efficiency, component sizing, and overall economic feasibility.

Hybrid OTEC systems integrated with desalination processes have been explored to enhance overall resource utilization and improve economic competitiveness (Azmi et al., 2024). In parallel, artificial intelligence models and multi-objective optimization techniques have been applied to optimize turbine parameters, condenser configurations, and overall system performance, often balancing thermal efficiency with economic indicators such as LCOE (Chung and Wu, 2024a, 2024b). Experimental and prototype-scale investigations, including 1 kW and 50 kW systems, have further validated thermodynamic modeling results and provided insights into real operational behavior (Lu et al., 2024; Zhang et al., 2025).

Beyond thermodynamic and component-level improvements, structural and mechanical aspects of the Cold Water Pipe (CWP) have received considerable attention. As the CWP connects surface platforms to deep cold seawater sources, its structural integrity is critical for safe and reliable operation (Al Kautsar et al., 2025). Finite element studies have optimized stiffening systems and reinforcement geometry to improve load resistance and bending performance (Rasgianti et al., 2024a). Coupled dynamic analyses have revealed significant interactions between floating platforms, mooring systems, and long CWPs in deep-water environments (Hisamatsu and Utsunomiya, 2024). Additionally, heat transfer along extended CWPs has been shown to increase cold seawater temperature before reaching the condenser, thereby reducing the effective thermal gradient (Firmansyah et al., 2024; Mao et al., 2023). These findings highlight that deeper intake depths may improve temperature differentials but simultaneously introduce structural, hydraulic, and thermal challenges.

From an economic standpoint, techno-economic assessments have evaluated capital expenditure (CAPEX), operational expenditure (OPEX), and Levelized Cost of Electricity (LCOE) for large-scale OTEC systems (IEA-OES, 2024; Langer and Blok, 2023). These studies consistently indicate that heat exchangers, seawater pipelines, and floating platforms dominate total investment costs. Earlier foundational works also acknowledge that deeper cold seawater sources provide greater temperature differences but increase installation complexity and lifecycle costs (Avery and Wu, 1994; Martel et al., 2012; Nihous, 2007). However, in many cases, intake depth is treated as a secondary parameter rather than as a primary techno-economic design variable.

Based on the literature review, the depth of cold seawater intake plays a crucial role in determining the temperature difference between surface and deep seawater, which directly influences the thermodynamic performance of OTEC systems. A larger temperature gradient enhances cycle efficiency, increases Annual Energy Production (AEP), and supports a stable Capacity Factor (CF). However, deeper intake depths require longer CWPs, resulting in higher structural demands, pumping power, and fabrication and installation costs. The selection of intake depth therefore represents a fundamental trade-off between thermal efficiency and infrastructure expenditure.

Although this trade-off has been widely recognized, comprehensive

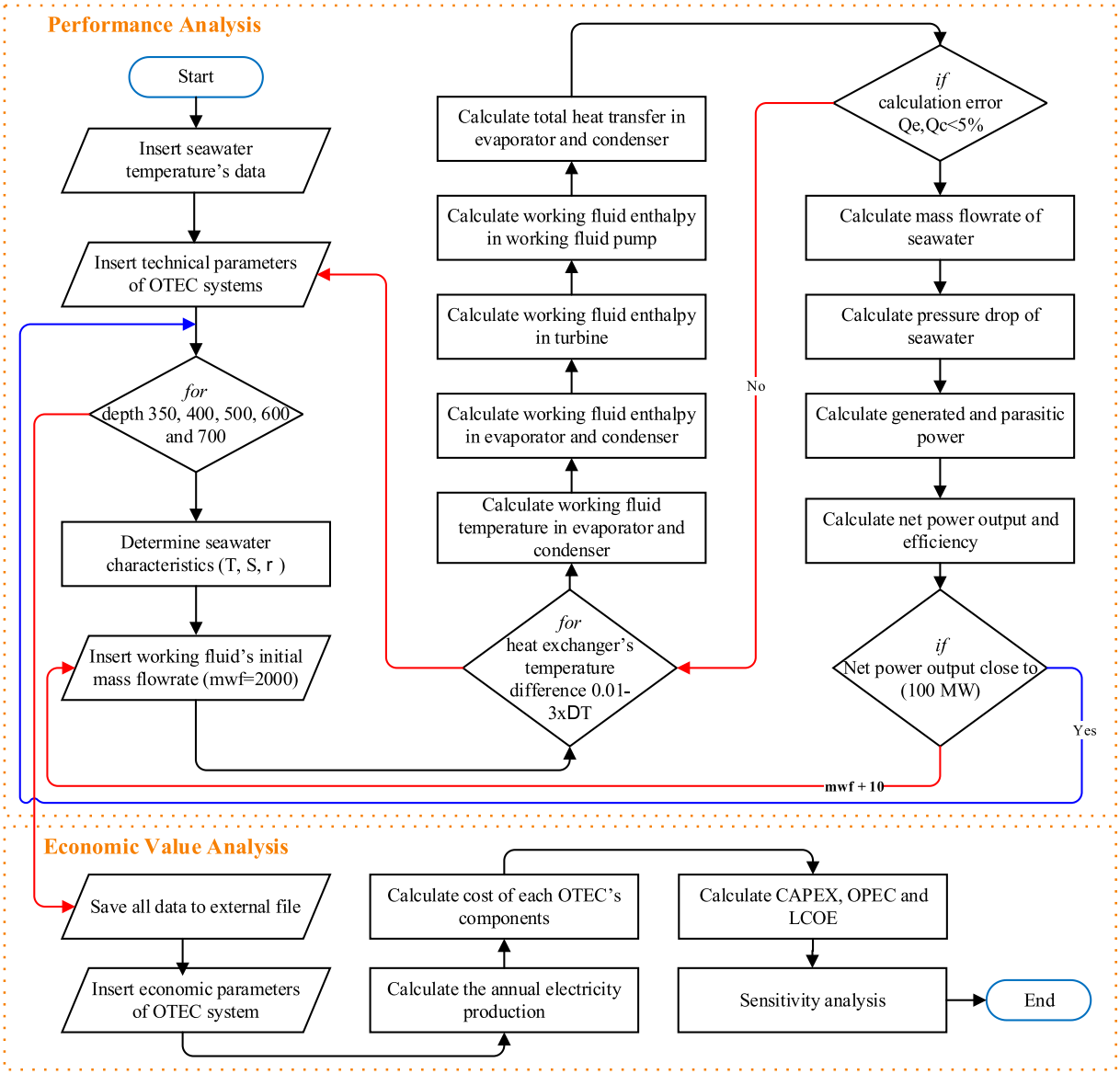

Fig. 2. Flowchart Analysis Steps.

depth-dependent analyses that simultaneously link vertical temperature profiles, mass flow requirements, component sizing, CAPEX structure, and LCOE remain limited, particularly for site-specific tropical environments. To address this gap, the present study provides a depth-resolved techno-economic assessment of OTEC feasibility in Manado Bay, Indonesia. Using HYCOM-derived vertical temperature profiles, five cold seawater intake depths (350, 400, 500, 600, and 700 m) are systematically evaluated within a closed Rankine cycle framework under a fixed 100 MW net power target. By explicitly linking intake depth to thermodynamic performance, component sizing, and LCOE outcomes, this study offers a site-specific perspective on intake-depth optimization and provides practical guidance for large-scale OTEC deployment in tropical coastal regions.

2. Methodology

2.1. Research flow

The performance of an OTEC system depends on several important factors, including system design, component efficiency, and environmental condition. The design process includes calculating mass and heat balance to ensure the system works properly (Cong et al., 2025). The choice of technology, such as heat exchangers, turbines, and working fluids, affects how efficiently the system converts energy. Additionally, the temperature difference between warm surface water and cold deep seawater acts as the main energy source, directly impacting the system's output (Langer et al., 2022). These factors together determine how well an OTEC system can operate.

To achieve the most optimized performance, the system must be analyzed based on key parameters such as capacity factor and energy production. (Shi et al., 2023). These values help measure how reliable and efficient the system is over time. However, performance alone is not enough—economic factors must also be considered. The financial feasibility of an OTEC system depends on investment costs, operational expenses, and the potential income from electricity production (Tobal-cupul et al., 2022). Since technical performance and economic viability are closely connected, they should be studied together to provide a complete evaluation.

There are different thermodynamic cycles that can be used for OTEC technology. In general, OTEC systems are divided into three types: Open Cycle, Closed Cycle, and Hybrid Cycle (Aresti et al., 2023). The Open Cycle uses seawater as both the working fluid and the energy source,

also producing fresh water as a byproduct. The Closed Cycle, in contrast, uses a separate working fluid, such as ammonia, which moves through a closed-loop system. The Hybrid Cycle combines features from both Open and Closed Cycles, improving efficiency and generating additional fresh water. Each system type has its own strengths and weaknesses, depending on its intended use and environmental conditions.

In this study, the Closed Rankine Cycle is chosen as the basis for performance calculations because of its efficiency, ability to be scaled up, and suitability for offshore applications. The research process follows a structured method, as shown in Fig. 2, which outlines the steps for performance analysis. This includes defining system parameters, running thermodynamic simulations, estimating energy output, and assessing financial feasibility. By following this approach, both technical and financial aspects are considered, allowing for a thorough evaluation of OTEC as a renewable energy solution.

The flowchart illustrates the step-by-step process for evaluating the performance and economic value of an OTEC system. The process begins with inserting seawater temperature data, followed by entering the technical parameters of the OTEC system. Since seawater characteristics vary with depth, data for 350, 400, 500, 600, and 700 m are considered. Depths below 350 m are excluded because the temperature difference between surface and deep seawater at those levels is still less than 20°C, which is insufficient to operate the OTEC system effectively. The initial mass flow rate of the working fluid is set, and the performance of the system is analyzed by calculating heat transfer in the evaporator and condenser, working fluid enthalpy, and temperature changes. To ensure the system meets the target net power output, a looping process is applied: if the calculated heat transfer in the evaporator and condenser does not result in the desired power output, the mass flow rate of the working fluid is increased incrementally by 10 in each iteration. This process continues until the power target is reached, ensuring efficient system performance under varying seawater conditions.

A key goal of the analysis is to achieve a net power output of approximately 100 MW. If the calculated power output is below this target, the mass flow rate of the working fluid is increased iteratively until the desired output is reached. Additionally, seawater flow rate and pressure drop are calculated to understand the energy consumption in the system. Any errors in the calculations, such as inconsistencies in heat transfer values, are corrected to improve accuracy. This iterative approach ensures that the model accurately represents the real-world performance of an OTEC system.

Once the system performance is determined, economic analysis is conducted. The collected data is stored, and economic parameters, such as capital expenditure (CAPEX) and operational expenditure (OPEX), are analyzed. The cost of each system component is calculated, and the annual electricity production is estimated. The Levelized Cost of Electricity (LCOE) method is used to assess the overall economic feasibility of the OTEC system. This approach helps determine whether the system is cost-effective and competitive compared to other renewable energy sources. Additionally, a sensitivity analysis is performed to evaluate the impact of changes in CAPEX and OPEX on the resulting LCOE, providing insights into the system's economic robustness.

2.2. Site description

The potential for renewable energy development from OTEC in Indonesia is significant due to its warm surface waters and deep cold seawater, which create the necessary thermal gradient for energy conversion. According to INOCEAN (2012), Indonesia has a theoretical OTEC resource of 4247,389 MW, but only a fraction is technically and practically feasible. The technical resource is estimated at 136,669 MW, while the practical resource—considering economic, environmental, and operational factors—is around 41,001 MW. These figures highlight Indonesia's potential for developing OTEC as a renewable energy source.

Several regions in Indonesia have deep-sea conditions suitable for OTEC, including the North Sulawesi Sea, North Bali, North Lombok, the Banda Sea, the Makassar Strait, and the Morotai Strait, as well as parts of Papua. These locations offer ideal conditions for OTEC power plants due to their stable temperature gradients. In this study, Manado Bay in North Sulawesi has been chosen as the case study site due to its deep waters and favorable oceanographic conditions, making it a promising location for assessing OTEC feasibility in Indonesia.

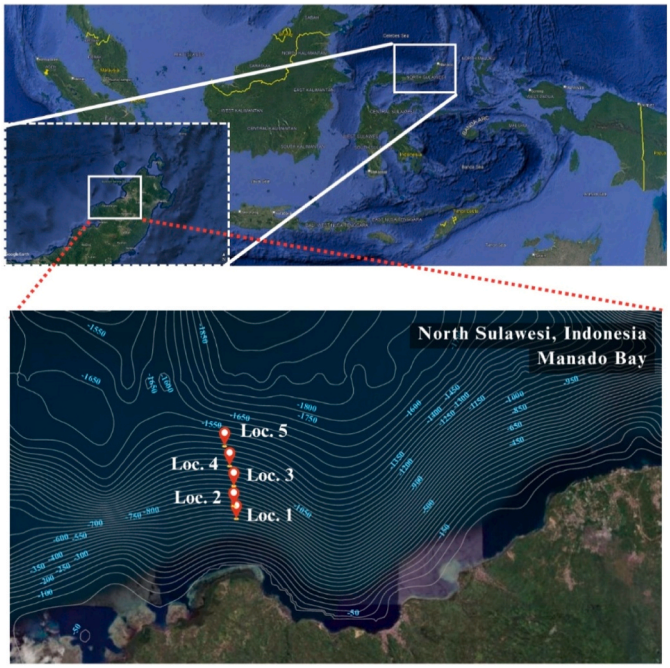

Fig. 3. Location Map in Manado Bay.

Table 1
Detail Locations.

Loc.	CWP Length	Coordinates		Distance to Shore
		Longitude	Latitude	
1	350 m	124.597886°	1.471397°	5.9 km
2	400 m	124.596653°	1.476390°	6.6 km
3	500 m	124.595634°	1.486041°	7.79 km
4	600 m	124.593364°	1.494449°	8.91 km
5	700 m	124.592016°	1.508962°	10.7 km

In determining the performance of the OTEC system in this report, the discussion focusing on three key parameters: net power output, cycle efficiency, and mass flow rate requirements. These parameters are evaluated based on different deep seawater depths, which directly impact the temperature difference used for energy conversion. A greater depth typically results in colder seawater, which can improve the system's efficiency by increasing the thermal gradient. This study considers five cold seawater depths—350, 400, 500, 600, and 700 m—to examine how variations in deep seawater temperature affect the overall performance of the OTEC system.

The temperature difference between surface and deep seawater plays a crucial role in determining the efficiency of the OTEC cycle. As the depth increases, the temperature of the deep seawater decreases, which enhances the thermal gradient and potentially improves energy conversion efficiency. However, using deeper seawater also presents challenges, such as increased infrastructure costs, particularly due to the longer CWP required. To better understand these factors, this report provides a detailed comparison of different seawater depths and their impact on system performance.

Fig. 3 and Table 1 present detailed information for each location,

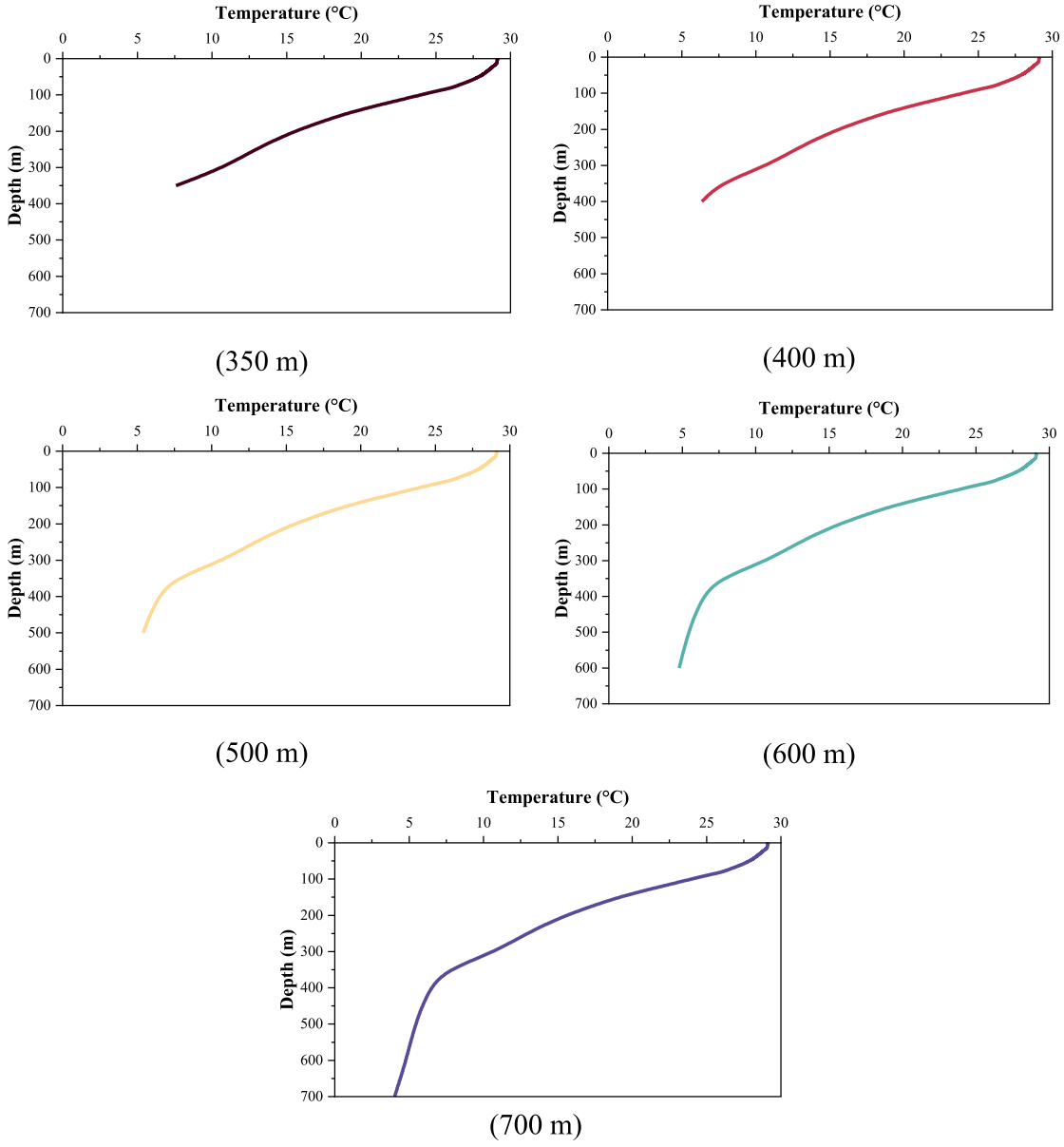

Fig. 4. Temperature Gradient for Each Location.

including temperature gradients and distances from shore, which range between 5 and 10 kilometers. Due to limitations in the available HYCOM data, the intake depth for cold seawater could not always match the seabed depth obtained from Indonesia's national bathymetric data. Instead, the selected locations were based on the closest available cold seawater intake depth from the dataset. Data were collected at multiple depth levels rather than relying on a single fixed depth, allowing for a more comprehensive analysis. This approach was adopted because the distance from shore influences the economic feasibility of OTEC systems, particularly in relation to energy transmission and infrastructure development. Fig. 4 illustrates seawater temperature variations at different depths, providing a clearer view of the potential efficiency gains and trade-offs when determining the optimal cold seawater intake depth for OTEC operations.

The temperature profiles used in this study are derived from HYCOM model outputs, which are widely applied in regional oceanographic assessments. While model-based datasets inherently involve a certain level of approximation compared to direct field measurements, they provide consistent spatial and vertical coverage that is suitable for preliminary techno-economic evaluation. This consistent dataset allows for a systematic comparison between locations and supports a robust assessment of thermal potential and economic feasibility.

Fig. 5 illustrates the temperature fluctuations observed at different water depths, specifically at 20 m (representing the intake for warm seawater), 350 m, 400 m, 500 m, 600 m, and 700 m (representing the intake for cold seawater). The data were collected over a one-year period, from January 1, 2023, to December 31, 2023. The figure reveals that temperature fluctuations occurred consistently throughout the year across all depths. These fluctuations were relatively minor, with variations of approximately 2°C. At a depth of 20 m, seawater temperatures ranged from 28.031°C to 30.162°C. At 350 m, temperatures varied between 6.758°C and 9.007°C. At 400 m, the range was from 5.905°C to 8.212°C, while at 500 m, temperatures fluctuated between 5.042°C and 6.988°C. At 600 m, the range narrowed to 4.343°C to 6.452°C, and at 700 m, it decreased further to between 3.540°C and 5.917°C.

Fig. 6 displays the annual variations in temperature differences measured at several depths designated for cold seawater intake. These temperature differences were calculated by subtracting the cold seawater temperatures from those recorded near the surface.

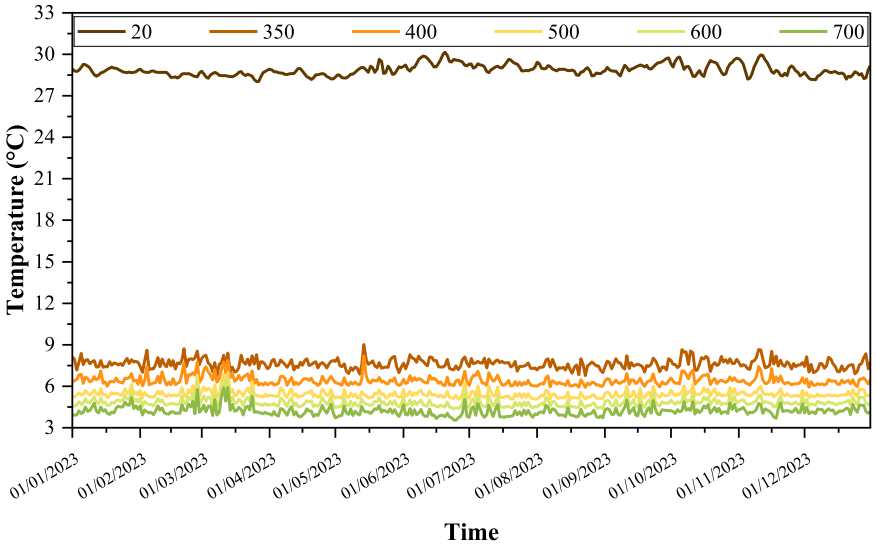

Fig. 5. Temperature Fluctuation.

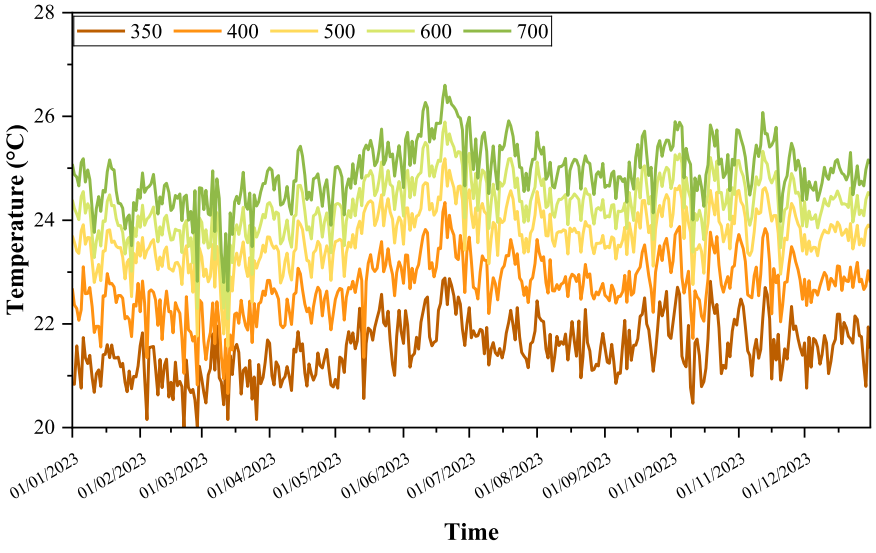

Fig. 6. Temperature Difference Fluctuation.

Throughout the year, all depths showed relatively consistent fluctuations, with slight increases or decreases depending on seasonal and environmental factors. At 350 m, the temperature difference ranged from 19.999°C to 22.884°C. At 400 m, the values were slightly higher, between 20.659°C and 24.339°C. Moving deeper, the range at 500 m extended from 21.563°C to 25.187°C. At 600 m, the temperature difference increased further, ranging from 22.099°C to 25.895°C. The largest differences were observed at 700 m, where values ranged from 22.634°C to 26.603°C. These figures indicate that, while temperature differences fluctuate over time, they remain within a relatively narrow band at each depth, providing useful data for evaluating cold water intake options.

In addition to the observed fluctuations, the annual average temperature differences at various depths provide a clearer view of the long-term thermal profile. At 350 m, the yearly average is 21.51°C, with monthly values ranging from 20.94°C to 22.08°C, indicating a typical variation of about ±0.57°C. At 400 m, the average rises to 22.72°C, while monthly differences fall between 21.98°C and 23.38°C, showing a fluctuation of approximately ±0.70°C. At 500 m, the annual average reaches 23.70°C, with monthly readings ranging from 23.01°C to 24.37°C, or roughly ±0.68°C. At 600 m, the average increases to 24.31°C, and monthly values range from 23.62°C to 25.08°C, giving a variation of about ±0.73°C. The highest average is found at 700 m, where the mean temperature difference is 24.93°C and monthly values range between 24.23°C and 25.79°C, resulting in a fluctuation of around ±0.78°C. These values offer insight into the stability and consistency of thermal conditions at depth throughout the year.

3. Assessment procedures

3.1. Technical assessment

The cycle performance of an OTEC system is based on how much heat can be extracted from seawater by the OTEC system. In the Rankine Cycle, the main responsibility of heat exchange is carried out by the heat exchanger. In the Rankine Cycle, two heat exchangers are used, which have different functions. One heat exchanger functions as an evaporator to convert the working fluid into saturated vapor form by utilizing seawater heat. While the other heat exchanger functions as a condenser which functions to convert the working fluid back into saturated liquid.

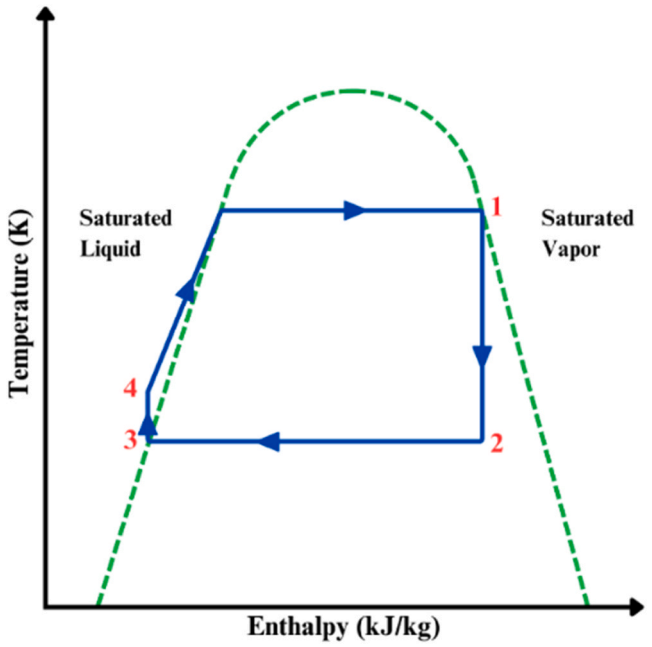

Fig. 7. Rankine Cycle Enthalpy-Temperature Flow Chart.

Total heat transfer in both heat exchangers can be calculated with the following equation:

$$Q_e = m_{WF}(h_1 - h_4) \quad (1)$$

$$Q_e = UA(\Delta Tm_e) \quad (2)$$

$$Q_e = m_{WS}c_{P,WS}(T_{wsi} - T_{wso}) \quad (3)$$

$$Q_c = m_{WF}(h_2 - h_3) \quad (4)$$

$$Q_c = UA(\Delta Tm_c) \quad (5)$$

$$Q_c = m_{CS}c_{P,CS}(T_{cso} - T_{csi}) \quad (6)$$

where:

$Q_{e,c}$ = Total heat transfer in evaporator and condenser (kW)
m_{WF}= mass flow rate work fluid (kg/s)
$m_{CS,WS}$ = mass flow rate cold seawater and warm seawater (kg/s)
h= Enthalpy of working fluid at each point (kJ/kg)
$c_{P,WS,CS}$ = Specific heat of seawater (kJ/kg.K)
$\Delta Tm_{e,c}$ = Temperature changes in the evaporator and condenser (K)
$T_{csi,o}$= Cold seawater temperature at condenser inlet and outlet (K)
$T_{wsi,o}$= Temperature of warm seawater at evaporator inlet and outlet (K)

The performance of the Rankine Cycle in the LPP system is strongly influenced by the temperature of the working fluid in the cycle. As shown in Fig. 7, the enthalpy value at each point in the Rankine Cycle is based on the working fluid temperature at each point. Where points 1 and 3 are working fluid conditions in the evaporator and condenser, while points 2 and 4 are in the turbine and working fluid pump.

The temperature of the working fluid in both heat exchangers (points 1 and 3) is determined using the Logarithmic Mean Temperature Difference (LMTD). Where the determination of the working fluid temperature using LMTD is calculated using changes in seawater temperature after passing through the heat exchanger. The calculation of the working fluid temperature at points 1 and 3 is formulated as Eqs. 7 and 8.

$$T_1 = \frac{e^{\left[\frac{T_{wsi}-T_{wso}}{\Delta Tm_e}\right]}T_{wso} - T_{wsi}}{e^{\left[\frac{T_{wsi}-T_{wso}}{\Delta Tm_e}\right]} - 1} \quad (7)$$

$$T_3 = \frac{e^{\left[\frac{T_{cso}-T_{csi}}{\Delta Tm_c}\right]}T_{cso} - T_{csi}}{e^{\left[\frac{T_{cso}-T_{csi}}{\Delta Tm_c}\right]} - 1} \quad (8)$$

$$T_{wso,cso} = T_{wsi,csi} - \Delta T_{e,c} \quad (9)$$

where:

$T_{1,3}$= Working fluid temperature at evaporator and condenser (K)

As shown in Fig. 7, the enthalpy values at points 1 and 3 are on the ideal working fluid enthalpy line. Therefore, the enthalpy value at these two points can be known by adjusting the temperature and thermodynamic properties of the working fluid. While the enthalpy values at points 2 and 4 are slightly outside the ideal working fluid line. On this basis, the enthalpy values at points 2 and 4 need to be calculated separately. The enthalpy value at point 2 is calculated by comparing the decrease in vapor quality after the working fluid has passed through the turbine (x_2). The calculation of the enthalpy of the working fluid after going through the turbine is formulated as follows:

$$s_{2i} = s_1 \quad (10)$$

$$x_2 = \left(s_2' - s_{2i}\right)/\left(s_2' - s_3\right) \quad (11)$$

$$h_{2i} = x_{2i}h_2' + (1 - x_{2i})h_3 \quad (12)$$

$$h_2 = h_1 - (h_1 - h_{2i})\eta_T \quad (13)$$

where:

s= Entropy of the working fluid at each point (kJ/kg.K)
v= Specific volume of working fluid at each point (m^3/kg)
η_T = Turbine Efficiency

The enthalpy of the working fluid at point 4, or after passing through the working fluid pump, is dependent on changes in working fluid pressure and pump efficiency. At point 4, the greater the working fluid pressure after passing through the pump, the greater the enthalpy value will be. The calculation of the working fluid enthalpy at point 4 is formulated by the following equation:

$$P_4 = P_1 \quad (14)$$

$$h_{4i} = h_3 + v_3(P_4 - P_3) \quad (15)$$

$$h_4 = h_3 + \frac{(h_{4i} - h_3)}{\eta_{P,WF}} \quad (16)$$

where:

$\eta_{P,WF}$ = Working fluid pump efficiency

In addition to the enthalpy value of the working fluid, the total net power output is also affected by the pressure drop of seawater while traveling through the pipe. The pressure drop is strongly influenced by the mass flow rate of seawater while traveling through the pipe. The determination of seawater mass flow rate requirements follows the heat transfer requirements to achieve the target system capacity. As demonstrated in Eqs. 3 and 6, seawater mass flow rate can be formulated as follows:

$$m_{WS,CS} = \frac{Q_{e,c}}{c_{P,WS,CS}\left(T_{wsi,cso} - T_{wso,csi}\right)} \quad (17)$$

The pressure drop calculation is done by comparing the pipe roughness coefficient factor with the pipe diameter. Where in this

report, the pipe roughness coefficient is calculated using the Colebrook equation as listed in Eq. 19.

$$\Delta P_H = f\frac{l_{WS,HE}\rho v^2}{2D} \tag{18}$$

where:

f = Pipe roughness coefficient factor

$$= \frac{1}{\sqrt{f}} = -2\log\left[\frac{2.51}{\mathrm{Re}_{WP}\sqrt{f}} + \frac{k}{3.7D}\right] \tag{19}$$

D = Pipe Diameter (m)

$l_{WS,CS}$= Length of seawater pipe (m)

Re_{WP} = Reynolds Number

k = Pipe roughness coefficient (m)

The calculation of net power output in OTEC is based on the amount of power generated by the generator (W_G) minus the amount of power needed to run the working fluid pump (W_P), warm seawater ($W_{P,WS}$), dan cold seawater ($W_{P,CS}$). Meanwhile, the efficiency value of the OTEC system is determined from the total net power output divided by the heat transfer in the evaporator. The calculation of net power output and efficiency of the OTEC system is formulated as follows:

$$W_{NET} = W_G - \left(W_{P,WF} + W_{P,WS} + W_{P,CS}\right) \tag{20}$$

$$\eta_{th} = \frac{W_{NET}}{Q_e} \tag{21}$$

$$W_G = m_{WF}(h_1 - h_2)\eta_T\eta_G \tag{22}$$

$$W_{P,WF} = m_{WF}(h_{4i} - h_3)/\eta_{P,WF}\eta_M \tag{23}$$

$$W_{P,CS} = m_{CS}\Delta P_{CS}/\rho_{CS}\eta_{P,SW} \tag{24}$$

$$W_{P,WS} = m_{WS}\Delta P_{WS}/\rho_{WS}\eta_{P,SW} \tag{25}$$

Furthermore, to calculate the exergy efficiency or the potential energy that can be utilized in the OTEC system, the following equation is used.

$$E_{x,OTEC} = \left(mc_p\right)_{ws} T_{wsi} + \left(mc_p\right)_{cs} T_{csi} \quad - \left[\left(mc_p\right)_{ws} + \left(mc_p\right)_{cs}\right] T_{wsi}^{\frac{\left(mc_p\right)_{ws}}{\left(mc_p\right)_{ws}+\left(mc_p\right)_{cs}}} T_{csi}^{\frac{\left(mc_p\right)_{cs}}{\left(mc_p\right)_{ws}+\left(mc_p\right)_{cs}}} \tag{26}$$

$$\eta_{ex,OTEC} = \frac{W_{NET}}{E_{x,OTEC}} \tag{27}$$

where:

$E_{x,OTEC}$= Exergy OTEC (kJ)

$\eta_{ex,OTEC}$= Exergy Efficiency OTEC (%)

$\left(mc_p\right)_{ws}$= $m_{WS} * c_{P\ WS}$

$\left(mc_p\right)_{cs}$= $m_{CS} * c_{P\ CS}$

Annual Energy Production (AEP) represents the total amount of electrical energy generated by the power plant over one year. In this study, the AEP is calculated using hourly net power output data derived from the thermodynamic simulation for each hour throughout the year. The hourly approach allows the model to capture temperature variations and their influence on system performance more accurately. The AEP is computed using Eq. (28):

$$AEP = \sum_{i=1}^{n}, W_{net}i \tag{28}$$

where $W_{net,i}$is the net power output at hour i, and $n$is the total number of operating hours in one year (8760 h).

After obtaining the AEP value, the Capacity Factor (CF) can be determined. The CF is an important indicator of plant performance, as it reflects the ratio between the actual annual energy produced and the maximum possible energy generation if the plant operates continuously at its rated capacity. A higher CF indicates that the plant operates closer to its design capacity over time, which generally implies better economic performance. Mathematically, CF is calculated using Eq. (29):

$$CF = \frac{AEP}{Rated\ Power\ x\ n}\ x \quad 100\% \tag{29}$$

where *Rated Power* is the nominal maximum output of the plant (100 MW in this study), and $n$is the total number of operating hours in a year.

Although the temperature fluctuations observed throughout the year are approximately 2°C, their impact on annual average efficiency is moderated by the relatively stable thermal gradient in tropical waters. Since the AEP calculation is based on hourly data, the influence of short-term temperature variations is inherently accounted for in the annual performance evaluation. As a result, the reported annual efficiency represents the integrated effect of these hourly variations rather than a single averaged temperature assumption.

Unlike the general system performance analysis, where key parameters are kept constant for comparison purposes, the economic analysis adopts a variable working fluid mass flow rate to ensure that the system at each intake depth achieves the target net power output of 100 MW. In addition, the heat exchanger surface area is adjusted according to the required thermal duty. As the cold seawater intake depth increases, the temperature difference becomes larger, reducing the required heat exchanger area and contributing to changes in overall system cost.

3.2. System configuration

The techno-economic performance of the Ocean Thermal Energy Conversion (OTEC) system is evaluated using a steady-state closed-cycle Rankine configuration with a target net power output of 100 MW. The system consists of an evaporator, turbine-generator unit, condenser, working fluid pump, and seawater pumping system. Ammonia (NH_3) is selected as the working fluid due to its favourable thermophysical properties for low-temperature applications, including high latent heat of vaporization and suitable saturation pressure within the typical OTEC operating temperature range. The thermodynamic properties of the working fluid are determined as functions of temperature and pressure within the numerical model.

The evaporator and condenser are modelled as shell-and-tube heat exchangers operating under steady-state conditions. Heat transfer in both components is evaluated using the Logarithmic Mean Temperature Difference (LMTD) method, and the overall heat transfer coefficient (U) is assumed constant at 4.5 W/m^{2}K to represent large-scale seawater heat exchangers operating in marine environments. The working fluid temperature at the evaporator and condenser outlets is determined based on seawater inlet–outlet temperature differences. Seawater flow is assumed

Table 2
Main Calculation Parameters.

Parameters	Symbols	Value
Generator efficiency (%)	η_G	95
Turbine efficiency (%)	η_T	95
Working fluid pump efficiency (%)	$\eta_{P,WF}$	85
Seawater pump efficiency (%)	$\eta_{P,SW}$	85
Thermal conductivity of heat exchanger (W/m^{2}K)	U	4.5
Depth of surface seawater (m)		10
Seawater velocity (m/s)		2
Maximum calculation difference (%)	Q_{error}	5
Seawater pipe material density-HDPE (kg • m^{-3})	ρ	995

Table 3
Validation Parameters (Kim et al., 2014).

Parameters	Symbol	Value
Power Generated by Generator (kW)	W_G	20
Net Power Output (kW)	W_{NET}	5.1
Warm seawater at evaporator inlet (K)	T_{wsi}	299.29
Warm seawater at evaporator outlet (K)	T_{wso}	296.25
Cold seawater temperature at condenser inlet (K)	T_{csi}	279.15
Cold seawater temperature at condenser outlet (K)	T_{cso}	282.25
Mass flow rate work fluid (kg/s)	m_{WF}	3.5
Mass flow rate warm seawater (kg/s)	m_{WS}	82
Mass flow rate cold seawater (kg/s)	m_{CS}	43
Warm Seawater Pump Power (kW)	$W_{P,WS}$	7.5
Cold Seawater Pump Power (kW)	$W_{P,CS}$	4.3
Thermal Efficiency (%)	η_T	2
Total heat transfer in evaporator (kW)	Q_e	1020
Working Fluid		R-32

incompressible, and pressure drop along the intake pipe is calculated using the Colebrook correlation to determine friction losses and pumping power requirements.

The performance calculation of the OTEC system is conducted using MATLAB software to ensure precise and reliable results. The calculation program is developed directly from the governing thermodynamic and heat transfer ensuring consistency with theoretical principles. MATLAB is employed to perform iterative numerical calculations, particularly for determining the working fluid mass flow rate required to achieve the fixed net power target under varying deep seawater depth conditions.

To make the analysis applicable to different scenarios, several configuration parameters are introduced to standardize the system across all evaluated conditions. Important factors such as turbine efficiency, generator efficiency, pump efficiencies, heat exchanger performance, seawater intake depth, and flow velocity are carefully considered to ensure realistic and practical results. A convergence tolerance of 5% (Q_{error}) is applied to ensure consistency in the energy balance between heat transfer calculations and thermodynamic state evaluations. The primary system parameters remain constant for all configurations and are summarized in Table 2.

In addition to the primary system parameters, which are kept constant for all configurations, this study also considers secondary environmental parameters that are varied according to the cold seawater intake depth. The main variable used in this variation is the deep seawater temperature, which changes with depth and geographical location. The temperature values presented in Section 2.2 are used as input data for each depth scenario in the simulation process. In this study, heat loss along the Cold Water Pipe (CWP) up to a depth of 700 m is assumed to be negligible due to the relatively stable deep-sea temperature profile and the high flow velocity, which limits heat transfer from the surrounding environment. This assumption is supported by previous studies stating that heat loss in CWP systems can be neglected when low thermal conductivity materials and adequate insulation are used (Firmansyah et al., 2024), which is consistent with the use of deep seawater pipes made of HDPE in this study due to its low thermal conductivity. The assumption is also considered valid for pipe depths of up to approximately 900 m) (Mukhtasor et al., 2024) as well as for moderate-length pipe configurations in computational OTEC studies (Aresti et al., 2025).

The analysis is conducted by varying the cold seawater intake depth to evaluate changes in system operating conditions. Temperature variations due to depth differences are incorporated into the calculation of the thermal gradient between surface and deep seawater, which serves as the basis for the thermodynamic performance analysis. This parameter is then integrated into the calculation of the working fluid thermodynamic states, required seawater mass flow rate, pumping power consumption, net power output, system efficiency, exergy efficiency, and the estimation of the levelized cost of electricity (LCOE).

The heat exchanger design is modeled by considering the available temperature difference for each depth scenario. The heat exchanger surface area is calculated based on the required heat transfer rate to achieve the target system capacity of 100 MW. With this approach, the methodology enables a systematic evaluation of different cold seawater intake depths within both thermodynamic and economic assessment frameworks of the OTEC system.

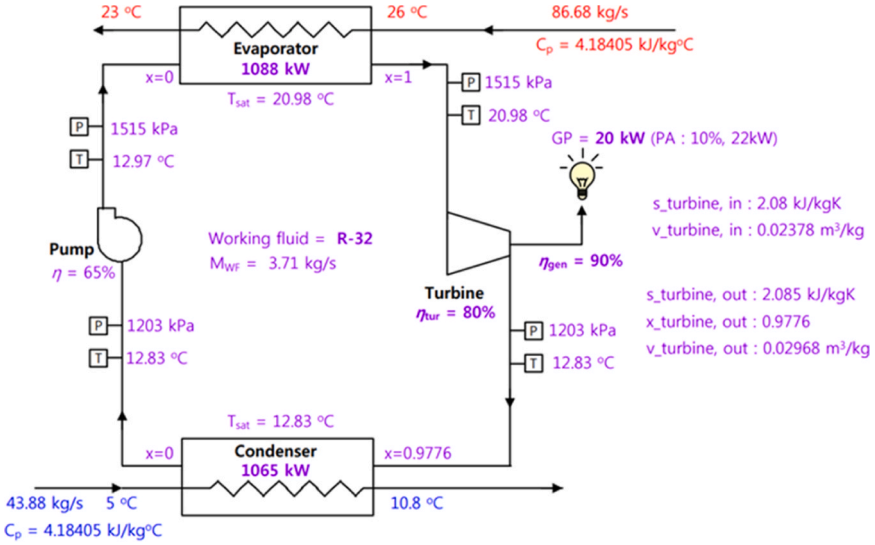

Fig. 8. Design thermodynamic heat cycle OTEC 20 kW (Kim et al., 2014).

Table 4
Validation Result.

Parameters	Symbol	Experiment	Numerical	Error (%)
Power Generated by Generator (kW)	W_G	20	18.9	5.50
Net Power Output (kW)	W_{NET}	5.1	5.1	0.00
Mass flow rate work fluid (kg/s)	m_{WF}	3.5	3.5	0.00
Mass flow rate warm seawater (kg/s)	m_{WS}	82	86	4.88
Mass flow rate cold seawater (kg/s)	m_{CS}	43	40	6.98
Warm Seawater Pump Power (kW)	$W_{P,WS}$	7.5	7.7	2.67
Cold Seawater Pump Power (kW)	$W_{P,CS}$	4.3	4.3	0.00
Total heat transfer in evaporator (kW)	Q_e	1020	1039	1.86

3.3. Numerical validation

Before being used for further analysis, the thermodynamic model developed in MATLAB was first validated to ensure the accuracy of the calculations. The validation process was conducted based on the study by (Kim et al., 2014), which investigated a single Rankine cycle OTEC system with a capacity of 20 kW through both numerical and experimental approaches. In that study, the numerical analysis was used as the basis for designing the OTEC system, which was later implemented as an experimental prototype. The main parameters used as validation references in this study were obtained from the experimental data presented in Table 3, particularly those related to power output and operating conditions. Several input parameters that were not explicitly available in the experimental report were determined based on the numerical analysis from the previous study, as illustrated in the thermodynamic diagram shown in Fig. 8. The design parameters applied in the validation process include a pump efficiency of 65%, a turbine efficiency of 85%, and a generator efficiency of 90%.

With the adjusted parameters, the numerical results presented in Table 4 show good agreement between the simulation outcomes and the experimental data. The error values obtained are below 10% for the main compared parameters, which is still within an acceptable range for thermodynamic system modelling. Therefore, the developed model can be considered validated and suitable for further analysis and extended studies. Furthermore, the validated thermodynamic diagram is presented in Fig. 9 to illustrate the consistency between the numerical results and the reference study.

3.4. Economic assessment

The significant financial investment required, particularly for each individual component, represents a significant obstacle to the advancement of OTEC systems. In general, OTEC cost elements fall into six major categories: (1) platform and mooring system, (2) generator, (3) heat exchanger, (4) seawater pipeline, (5) power transmission, (6) installation (Upshaw, 2012). To date, no industrial-scale OTEC systems have been successfully developed. The few OTEC power plants that have been successfully operated have only reached pilot capacity, such as the 105 kW Makai OTEC (Makai Ocean Engineering, 2020), OTEC 100 kW in Okinawa (Liu et al., 2020), as well as KRISO 1 MW OTEC (G. Peterson and Ju Kim, 2020).

Although capital expenditure (CAPEX) is incurred only at the initial construction of an OTEC system, it represents the highest investment value of OTEC systems. Despite the absence of OTEC plants on an industrial scale, some researchers have attempted to estimate the CAPEX value, particularly at a capacity of 100 MW. However, it should be noted that the existing costs are only estimates, and thus, in this study, additional costs are used to determine the CAPEX value. Consequently, the $CAPEX_{tot}$ (USD) value can be determined using Eq. 30.

$$CAPEX_{tot} = CAPEX \times (1 + ext_{CAPEX}) \tag{30}$$

where:

ext_{CAPEX} = Extra cost on CAPEX (%)

In addition to capital expenditure (CAPEX) costs, the investment costs of an OTEC system also include the costs of daily operations, maintenance, repair, and replacement of components, as well as labour and supervision costs, which are represented as operational expenditure (OPEX). The OPEX (USD) value is the most challenging economic value to quantify for industrial-scale OTEC systems. Based on this, some researchers propose that OPEX can be evaluated as a percentage of CAPEX. Some researchers argue that OPEX has a value ranging from 1.4% (Straatman and van Sark, 2008) and 2% (Oko and Obeneme, 2018) of CAPEX.

As illustrated in Fig. 2, an economic value analysis was conducted

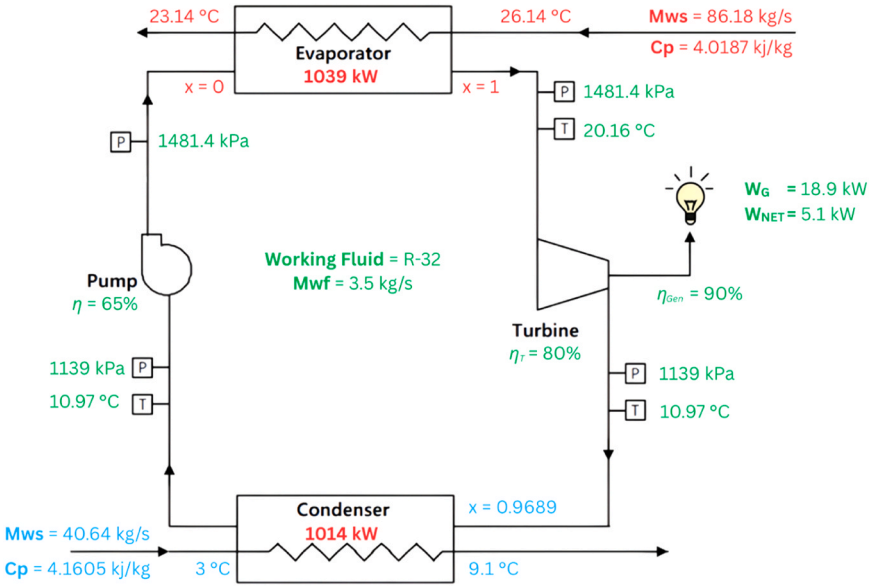

Fig. 9. Cycle Diagram Validation Result of OTEC 20 kW.

Table 5
Price Parameters of Each Component of The OTEC System.

Parameters	Price	Scale	Ref. Size	Ref.
Turbine (USD/ kW_{gross})	393	0.6	136	(Bernardoni et al., 2019); (Langer and Blok, 2024)
Heat exchanger (USD/m2)	271	0.84	80	(Langer and Blok, 2024)
Pump (USD/ kWpump)	1674	–	–	(Saadha et al., 2025)
Sea Water Pipe (USD/ (kg_{pipe}))	9	–	–	(Langer and Blok, 2024)
Platform (USD/ kWgross)	5359.45	0.35	28.1	(Bernardoni et al., 2019)
Deployment (USD/ kWgross)	876	–	–	(Langer and Blok, 2024)
Power Transmission (USD/kWgross)	10.3*D + 68.7		–	(Bosch et al., 2019)
Design & Management (USD/kWgross)	3736	0.3	4	(Bernardoni et al., 2019); (Langer and Blok, 2024)
Extra Costs (% CAPEX)	3			(Saadha et al., 2025)
OPEX (%CAPEX/ year)	3			(Saadha et al., 2025)
Discount rate (%)	10			(Lu et al., 2025)

employing the levelized cost of electricity (LCOE) comparison method to evaluate the economic value of OTEC systems with varying seawater depths. LCOE (USD cent) is the minimum average price at which electricity needs to be sold to reach equilibrium with all project expenditures at the end of its useful life (Visser and Held, 2014). In addition to the previously described CAPEX and OPEX, the determination of the LCOE value also employs the capital recovery factor parameter and annual electricity production per year. The calculation of the LCOE value is formulated as Eq. 31.

$$LCOE = \frac{CRF \times CAPEX_{tot} + OPEX}{AEP} \tag{31}$$

where:

CRF= Capital recovery factor

AEP= Annual electricity production (MW/year)

The capital recovery factor (*CRF*) value for OTEC system is affected by the discount rate, as shown in Eq. 28. When calculating LCOE, the discount rate (*dr*) can have a substantial effect on the outcome. In addition to the discount rate, the projected life of the plant also determines the CRF value of the OTEC system. In this study, a projected life of 30 years is used.

$$CRF = \frac{dr(1+dr)^n}{(1+dr)^n - 1} \tag{32}$$

where:

n= Projected life of the plant (year)

dr= Discount rate (%)

To model the cost of each component, several researchers have applied component-based cost estimation combined with scaling relationships to determine CAPEX and OPEX for LCOE calculation. Large-scale techno-economic studies use cost-scaling approaches to relate equipment cost with plant capacity, pipeline length, pumping depth, and thermal resource characteristics, allowing estimation of LCOE across different regions and plant configurations (Langer and Blok, 2024). In regional case studies, advanced data analytics and machine learning have also been used to forecast long-term temperature profiles and support economic evaluation, including LCOE and payback period estimation in specific geographic contexts (Rashid et al., 2024).

Recent work has further integrated thermo-economic and exergoeconomic frameworks to allocate costs to individual components based on exergy destruction and capital investment distribution (Ciappi et al., 2024; Lu et al., 2025). These frameworks enable identification of the most cost-intensive subsystems, such as heat exchangers, pipelines, and pumping units, and support targeted optimization strategies to improve both technical performance and economic feasibility. In addition, component cost and scaling models have been coupled with techno-economic assessments of combined systems, such as OTEC-SWAC integration, revealing the effects of design parameters like pipeline length and temperature gradients on LCOE (Saadha et al., 2025).

Following these established approaches, the present study determines the economic value of each OTEC component using reference prices obtained from previously published sources. The component cost breakdown and corresponding references are summarized in Table 5, together with the parameters used for LCOE calculation. All component costs are expressed in USD for the year 2026 to ensure consistency throughout the analysis.

4. Results and discussion

4.1. System performance

The results of the OTEC system performance analysis under different deep seawater intake depths show a clear relationship between intake

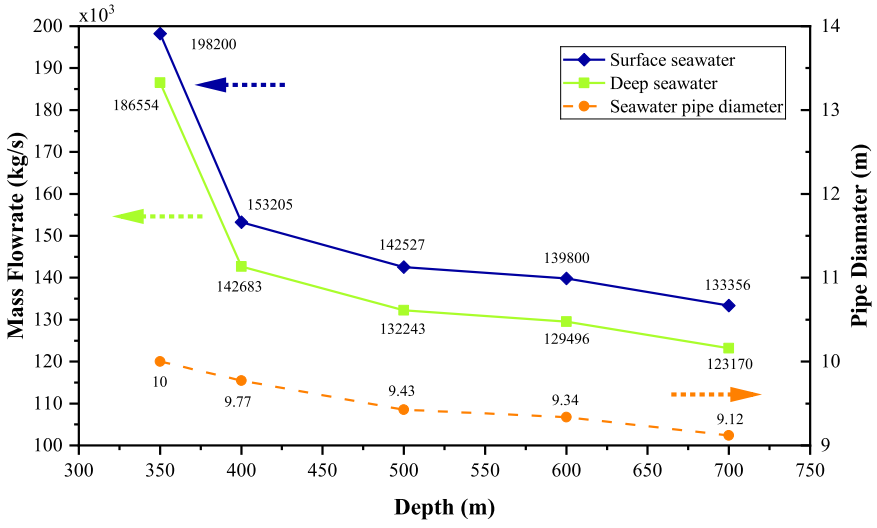

Fig. 10. The Results of The Mass Flow Rate Requirement and Seawater Pipe Diameter of The OTEC System Based on Seawater Depth.

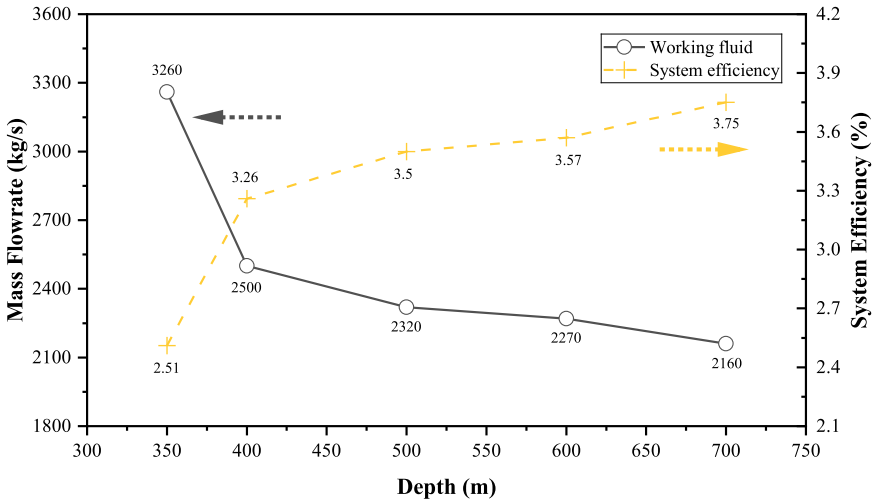

Fig. 11. Results of Efficiency and Working Fluid's Mass Flow Rate of The OTEC System Based on Seawater Depth.

depth and the main operational parameters of the system. As the depth of cold seawater increases, the temperature difference between surface and deep seawater becomes larger (see Fig. 6), which directly reduces the required seawater mass flow rate. As shown in Fig. 10, both surface and deep seawater mass flow rates decrease consistently with increasing intake depth. This condition occurs because a higher thermal gradient improves the effectiveness of heat transfer in the heat exchangers, allowing the required thermal energy to be obtained with a smaller volume of seawater while still achieving the targeted power capacity.

The figure also shows that, at every depth, the required mass flow rate for surface seawater is consistently higher than that for deep seawater. A particularly notable difference is observed when comparing systems using cold water intake from 350 m and 400 m depths. The mass flow rate for surface seawater drops by around 45,000 kg/s, while that of deep seawater decreases by approximately 44,000 kg/s. Beyond 400 m, the changes become less significant. Between 400 m and 700 m, the surface seawater mass flow rate decreases by only about 20,000 kg/s, and the deep seawater flow rate reduces by around 9000 kg/s. This indicates that although deeper intakes offer improvements, the most substantial gains occur between shallower depths. This trend suggests that the temperature reduction of deep seawater becomes progressively smaller beyond 400 m, resulting in diminishing increments of the thermal gradient. Consequently, the thermodynamic driving force for heat transfer does not increase proportionally at greater depths, leading to a reduced rate of performance improvement.

In line with the changes in mass flow rate, the required seawater pipe diameter also decreases as deeper seawater is utilized. The pipe diameter is determined based on the mass flow rate, considering a constant seawater flow velocity of 2 m/s. Since a lower mass flow rate requires a smaller volume of seawater to be transported, the pipe size must be adjusted accordingly. However, despite the variation in mass flow rates, the reduction in pipe diameter remains relatively small, with a maximum difference of less than 1 m between different depth configurations. For instance, the difference in pipe diameter between systems using deep seawater intake depths of 400 m and 500 m is only 0.09 m, which is quite minimal. This indicates that while deeper seawater reduces the required mass flow rate, it does not significantly impact the infrastructure size, making deeper seawater an attractive option for OTEC applications.

The depth of seawater used in an OTEC system plays a crucial role in determining its efficiency and overall performance. As shown in Fig. 11, system efficiency increases with deeper intake of cold seawater. This pattern emerges because a larger temperature difference between surface and deep seawater enhances the heat exchange process, enabling more effective energy conversion. At a depth of 350 m, the system reaches an efficiency of 2.51%. This value rises sharply to 3.26% at 400 m, marking a significant improvement. Beyond this point, the increase becomes more gradual, with efficiencies of 3.50%, 3.57%, and

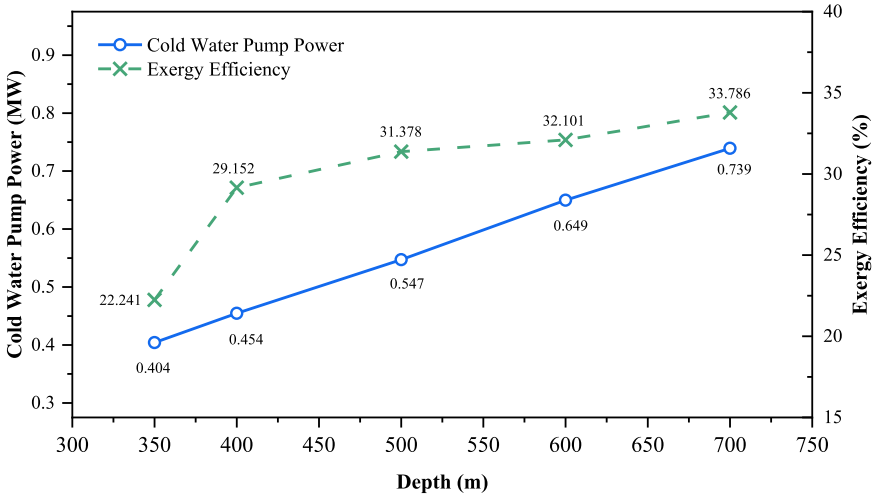

Fig. 12. Results of Exergy Efficiency and Cold Water Pump Power of The OTEC System Based on Seawater Depth.

Table 6
Summary of Component Sizes.

Component	Depth (m)				
	350	400	500	600	700
Net Power Output (MW)	100.02	100.28	100.08	100.14	100.22
Power gross (MW)	102.34	102.27	102.16	102.29	102.44
Evaporator area (m^2)	335000	305000	275500	240500	232500
Condenser area (m^2)	335000	305000	275500	240500	232500
Working fluid pump power (MW)	1.44	1.42	1.42	1.39	1.37
Surface seawater pump power (MW)	0.23	0.12	0.11	0.11	0.11
Deep seawater pump power (MW)	0.65	0.45	0.55	0.65	0.74
Warm seawater mass flowrate (kg/s)	198200	153205	142527	139800	133356
Warm Seawater pipe diameter (m)	10	9.77	9.43	9.34	9.12
Warm seawater pipe length (m)	20	20	20	20	20
Cold seawater mass flowrate (kg/s)	186554	142683	132243	129496	123170
Cold seawater pipe diameter (m)	10	9.40	9.05	8.96	8.74
Cold seawater pipe length (m)	350	400	500	600	700
Seawater pipe thickness (m)	0.09	0.09	0.09	0.09	0.09
Seawater pipe density (kg/m^3)	995	995	995	995	995
Warm seawater pipe weight (kg)	113038.24	110481.61	106586.39	105560.91	103110.54
Cold seawater pipe weight (kg)	1978169.24	2126601.47	2559531.96	3039411.32	3458614.76
Mass flowrate working fluid (kg/s)	3260	2500	2320	2270	2160

3.75% at depths of 500 m, 600 m, and 700 m respectively. The diminishing efficiency gain beyond 400 m can be explained by the stabilization of deep seawater temperature at greater depths. While the initial increase in depth significantly enlarges the thermal gradient, further depth increments provide only marginal additional temperature differences. Since OTEC efficiency is fundamentally limited by the available temperature difference, the thermodynamic benefit obtained from deeper intake depths gradually decreases. These improvements, though incremental, are meaningful for OTEC systems, as even slight efficiency gains can lead to increased energy output and improved operational reliability. The clear positive correlation between efficiency and intake depth suggests that utilizing deeper seawater can be beneficial for maximizing power generation, as long as technical feasibility and economic considerations are also taken into account.

On the other hand, the mass flow rate requirement for the working fluid decreases as the depth of deep seawater increases. This inverse relationship occurs because improved system efficiency reduces the amount of working fluid needed to produce the same level of power output. As shown in Fig. 11, the working fluid mass flow rate at a depth of 350 m is approximately 3260 kg/s, then drops significantly to around 2500 kg/s at 400 m. Compared to the seawater mass flow rate, which shows larger variations across depths, the reduction in working fluid flow becomes relatively minor beyond 400 m. This behaviour is consistent with the observed efficiency trend, where the major thermodynamic improvement occurs between 350 m and 400 m, while deeper intakes contribute only incremental performance gains. However, optimizing this parameter remains important, as the working fluid flow rate directly affects the size and cost of heat exchangers, turbines, and other key OTEC components. By selecting an appropriate deep seawater intake depth, the system can maintain a balance between improved efficiency and reduced working fluid requirements, supporting a more sustainable and cost-effective OTEC operation.

In addition, the depth of cold seawater intake also affects the required pumping power of the cold seawater pump. In general, the pump power demand shows an increasing trend as the intake depth increases. This can be observed at a depth of 400 m, where the pump power requirement is 0.454 MW, and it increases to 0.547 MW at greater depths (see Fig. 12). The trend indicates an almost linear increase with depth. This occurs because a deeper intake requires a higher pump head to deliver seawater to the surface, resulting in greater power consumption.

On the other hand, the depth of deep seawater intake also influences the exergy efficiency of the system. As shown in Fig. 12, the exergy efficiency at 350 m is 22.241%, then increases significantly to 29.152% at 400 m, and continues to rise to 33.786% at 700 m. The improvement in exergy efficiency is mainly affected by the lower temperature of deep seawater at greater depths and the reduced mass flow rate requirement. As the intake depth increases, the deep seawater temperature becomes lower, leading to a larger temperature difference (ΔT) between surface seawater and cold seawater. This condition enhances the thermal energy utilization of the system. In addition, the lower required mass flow rate allows the available energy to be used more effectively, resulting in higher exergy efficiency.

The significant increase in efficiency between 350 and 400 m is

Table 7
Estimated Cost for Each Component in Thousand USD, 2026.

Parameters	Depth (m)				
	350	400	500	600	700
Turbine	11928.74	11924.22	11916.48	11925.54	11936.18
Evaporator	87277.52	79469.66	71795.68	62661.93	60563.13
Condenser	87277.52	79469.66	71795.68	62661.93	60563.13
Working fluid pump	2412.71	2380.31	2374.42	2322.35	2299.70
Surface seawater pump	196.57	196.57	189.58	187.77	183.39
Deep sea water pump	1095.11	761.08	915.93	1087.69	1237.64
Surface seawater pipe	994.33	994.33	959.28	950.05	927.99
Deep Sea water pipe	17803.52	19139.41	23035.79	27354.70	12796.87
Platform	236751.49	236699.12	236609.45	236714.36	236837.59
Installations	89648.36	89591.71	89494.78	89608.20	89741.54
Design & Management	39523.95	39516.46	39503.62	37392.50	39536.27
Power Transmission	30.16	45.70	53.99	62.28	70.57
Total	**574939.97**	**560188.21**	**548644.68**	**532929.29**	**516694.02**

Table 8
The Results of The Calculation of The Economic Value of The OTEC System at Each Depth.

Parameters	Depth (m)				
	350	400	500	600	700
Net Power Output (MW)	100.02	100.28	100.08	100.14	100.22
Power gross (MW)	102.34	102.27	102.16	102.29	102.44
Project life time (year)	30	30	30	30	30
Extra Costs (%CAPEX)	3	3	3	3	3
OPEX (%CAPEX/year)	3	3	3	3	3
Discount rate (%)	10	10	10	10	10
CRF	0.11	0.11	0.11	0.11	0.11
CF (%)	99.98	99.92	99.51	99.44	99.43
AEP (MWh)	875882.6	869866.4	871762.7	871135.7	871068.6
CAPEX (USD, 2026)	**592188.2**	**576993.9**	**565104.0**	**548917.2**	**532194.8**
OPEX (USD, 2026)	**17765.6**	**17309.8**	**16953.1**	**16467.5**	**15965.8**
LCOE (USD cent, 2026)	**9.20**	**9.03**	**8.82**	**8.57**	**8.31**

* in thousand dollars except for LCOE

mainly due to the considerable drop in deep seawater temperature within this depth range. Beyond 400 m, the temperature decrease becomes more gradual, so the exergy efficiency continues to increase but at a slower rate, as previously discussed.

4.2. Economic value

4.2.1. Component size and cost

After completing the performance analysis, the next step is the economic evaluation, which begins by estimating the component sizes needed to achieve a net power output of 100 MW. The calculation results are shown in Table 6, covering component dimensions at deep seawater intake depths of 350, 400, 500, 600 and 700 m. The most notable difference appears in the heat exchanger areas, both for the evaporator and condenser, where at 350 m—the depth with the smallest temperature difference—larger heat exchanger sizes are required to meet the same power target. At this depth, the mass flow rates of the working fluid, warm seawater, and cold seawater are also higher. In contrast, at 700 m, the most significant variation is found in the estimated weight of the cold water pipe, which increases along with the depth. These variations in component sizes and characteristics ultimately result in different CAPEX values across each depth scenario.

Once the size of each component needed to achieve the target net power output of 100 MW has been determined, the next step is to estimate the cost of each component, which will be used to calculate the total CAPEX. The cost estimation is based on the component size in Table 6 and the unit price references listed in Table 5. The estimated cost for each component is presented in Table 7. As shown in the table, and as previously discussed, the system at a depth of 350 m requires a larger heat exchanger area, which makes the cost of that component significantly higher than at other depths. For most other components, the cost increases slightly with greater depth. Similarly, for the Cold Water Pipe (CWP), the increase in depth directly raises the estimated structural weight, resulting in higher costs as depth increases. This leads to a more significant contribution of pipe cost in configurations with greater intake depths.

4.2.2. LCOE calculation

The economic analysis of the OTEC system highlights an important trend: as the depth of seawater intake increases, both the capital expenditure (CAPEX) and the levelized cost of electricity (LCOE) decrease. This indicates that utilizing deeper seawater sources offers a more cost-effective solution for power generation, even though certain components such as deep seawater pumps and pipes may require slightly higher investments.

As shown in Table 8, the CAPEX at a depth of 700 m is significantly lower than at shallower depths, with a reduction of 60 million USD compared to the 350 m system. The CAPEX reduction between 350 m and 400 m as well as between 600 m and 700 m is relatively small, around 16 million USD. In contrast, the reductions between 400 m and 500 m, and between 500 m and 600 m, amounting to 11 million USD and 17 million USD. These differences suggest that the most impactful cost savings occur within specific depth ranges. This pattern indicates that the economic performance of the system is highly sensitive to depth-dependent thermal improvements within certain intervals, rather than responding linearly to increasing intake depth. The non-uniform reduction in CAPEX reflects the combined influence of thermodynamic efficiency gains and component sizing requirements, particularly in the heat exchange system.

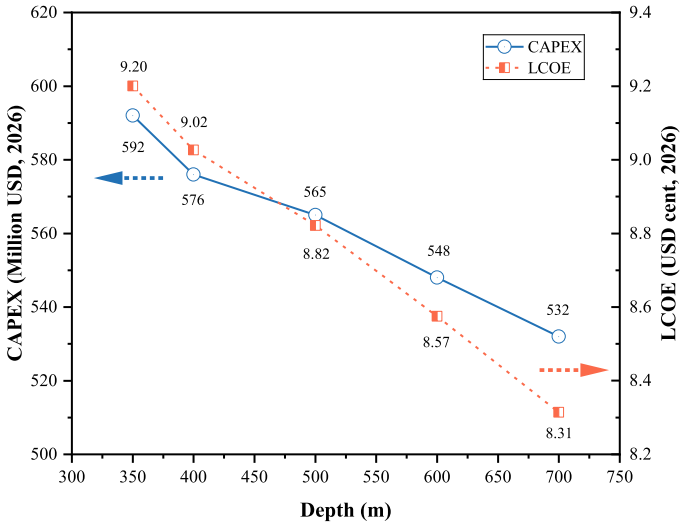

Fig. 13. Difference in CAPEX and LCOE Values at Each Depth.

The overall decline in CAPEX is primarily attributed to the reduced cost of key thermal components, particularly evaporators and condensers (see Table 7), which are critical to the energy conversion process in OTEC systems. Although some elements, such as the platform, installation, and management costs, tend to slightly increase with depth (as also indicated in Table 7), the general CAPEX trend continues to decrease. This suggests that reductions in heat exchanger size and associated working fluid flow requirements have a stronger economic impact than the incremental structural costs associated with deeper installations. In other words, the thermodynamic benefits gained from increased temperature differences outweigh the additional mechanical and installation costs. This analysis reinforces the importance of optimizing the selection and configuration of thermal exchange components to enhance the financial feasibility of OTEC power plants.

The LCOE, which represents the cost of generating electricity over

Table 9
CAPEX and OPEX Variation Scenarios.

Parameters	Variation
CAPEX adjustment (%)	-20, −15, −10, −5, 5, 10, 15, 20
OPEX (%CAPEX)	2, 4, and 6

the lifetime of the plant, also follows a decreasing pattern with increasing seawater depth. Although the reduction in LCOE from 350 m to 700 m is approximately 0.9 USD cent/kWh, this difference corresponds to nearly 10% of the total LCOE. When projected over the plant lifetime and large-scale electricity production, the cumulative economic impact becomes substantial. A lower LCOE implies that the plant can generate electricity at a more competitive price, making OTEC a more attractive renewable energy option for commercial implementation. However, the gradual reduction in LCOE at greater depths indicates diminishing economic returns, as the additional efficiency gains become progressively smaller. Since net power output remains relatively constant across depths, the primary driver of LCOE reduction is the decrease in capital cost rather than a substantial increase in annual energy production.

Fig. 13 illustrates the trend of decreasing LCOE and CAPEX values with increasing seawater intake depth. The most significant reduction in LCOE occurs between deep seawater intake depths of 400 m to 500 m

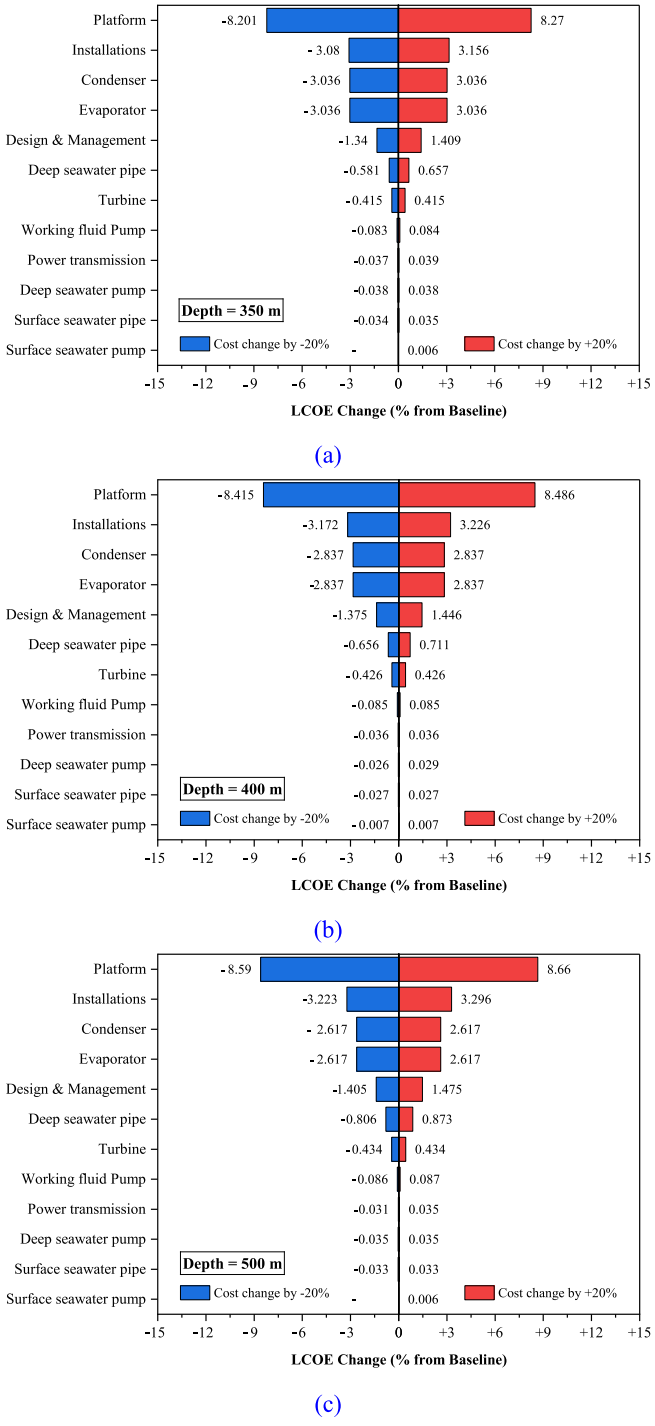

Fig. 14. Effect of Cost Component Changes at Different Water Depths: (a) 350 m; (b) 400 m; (c) 500 m; (d) 600 m; and (e) 700 m.

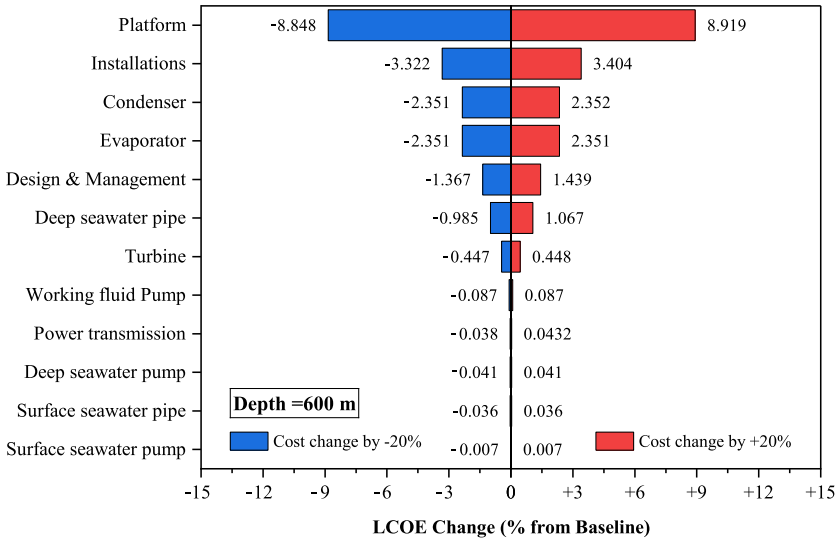

(d)

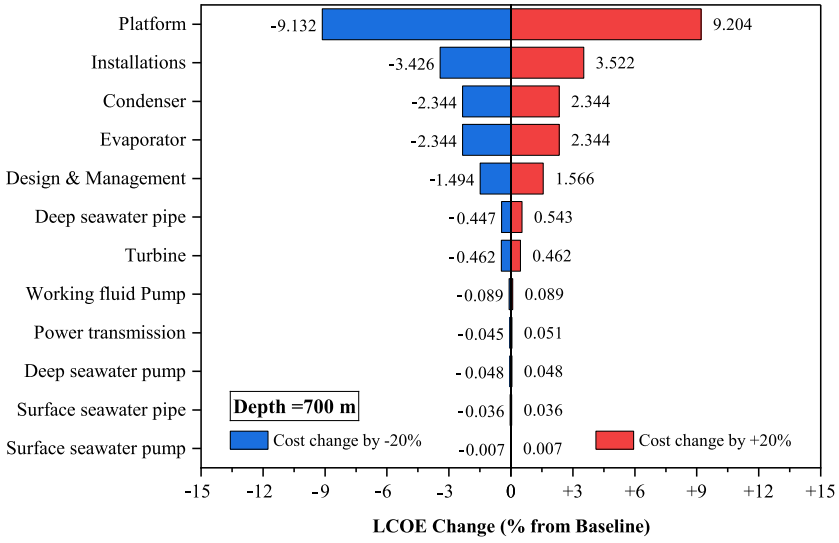

(e)

Fig. 14. (*continued*).

and 500 m to 600 m. This reduction is primarily driven by an increase in the annual energy production at 500 m depth (see Table 9), which enhances the denominator in the LCOE calculation (Eq. 31) and thereby lowers the resulting value.In contrast, the reduction in LCOE between 350 m to 400 m and 600 m to 700 m is relatively smaller due to the limited CAPEX difference observed in those intervals. The figure also shows that the CAPEX reduction rate remains relatively consistent across increasing depths. These findings suggest the presence of an economically favorable depth range, beyond which further increases in intake depth provide only marginal financial improvement. Therefore, the optimal design depth should be determined not solely based on maximum efficiency, but on the balance between thermodynamic gains and incremental investment costs.

4.2.3. *Sensitivity analysis*

4.2.3.1. Components cost sensitivity. In this analysis, the investment cost of each component was varied by ±20%, while the other components were maintained at their baseline values during each variation. This procedure was applied individually to all main components and repeated for all investigated deep seawater depths, namely 350 m, 400 m, 500 m, 600 m, and 700 m. The purpose of this analysis was to evaluate the influence of each component on the LCOE and to identify the components with the strongest impact. The results are presented in the tornado charts in Fig. 14.

The results show that the platform cost is the most influential component at all water depths. A ± 20% change in platform cost leads to approximately ±8% to ±9% variation in LCOE. This impact is significantly larger than that of any other component. In addition, the effect slightly increases as the water depth becomes deeper, with the highest influence observed at 700 m. This trend can be explained by the higher structural requirements and material usage needed for deeper installations, which increase the overall capital cost of the platform.

The second most influential components are installation, condenser, and evaporator. A ± 20% variation in installation cost results in about ±3% to ±3.5% change in LCOE. The influence of installation cost also slightly increases with depth, likely due to more complex offshore operations in deeper waters. The condenser and evaporator show similar

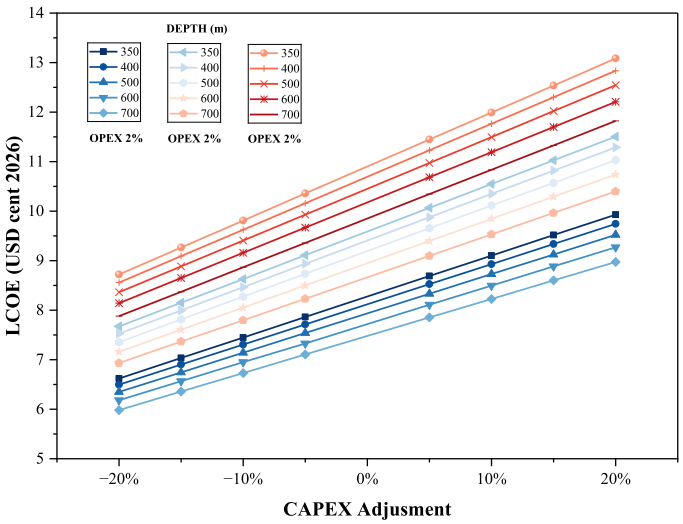

Fig. 15. Effect of CAPEX Adjustment on LCOE.

levels of sensitivity, generally between ±2.3% and ±3.0%. Since these components are part of the main thermodynamic system, their cost has a noticeable effect on the overall project economics.

Design and management cost has a moderate impact, contributing around ±1.3% to ±1.5% variation in LCOE. In contrast, the other components, including the deep seawater pipe, turbine, working fluid pump, power transmission system, deep seawater pump, and surface seawater system, show relatively small effects. Even with a ± 20% cost change, their impact on LCOE is generally below ±1%. Although the influence of the deep seawater pipe slightly increases with water depth, its contribution remains much lower compared to the platform and installation costs.

Overall, the ranking of component sensitivity remains consistent across all water depths. The results indicate that the LCOE is mainly driven by structural and major capital components, especially the platform. Therefore, efforts to reduce LCOE should primarily focus on optimizing platform design and installation strategies, as these offer the greatest potential for cost reduction.

4.2.3.2. CAPEX and OPEX sensitivity. To further examine the effect of CAPEX and OPEX changes on the LCOE, a sensitivity analysis was carried out by applying several variations to both parameters, as shown in Table 9. The table presents eight levels of CAPEX variation. Each percentage is multiplied by the original CAPEX value from Table 6 at each depth, and the result is added to the original value to obtain the adjusted CAPEX. For example, a 20% increase means that 20% of the original CAPEX is added to its base value. Meanwhile, the OPEX values are calculated as percentages of the adjusted CAPEX. A cross-combination of these variations was then performed, resulting in a total of 24 different scenarios.

The results of the sensitivity analysis are shown in Fig. 15 and Fig. 16. Fig. 15 focuses on the effect of CAPEX variation on the LCOE, while Fig. 16 illustrates the influence of changes in OPEX. In Fig. 11, it can be clearly seen that the LCOE increases steadily as the CAPEX adjustment becomes higher. Each step of CAPEX increase, whether 5%, 10%, 15%, or 20%, results in a noticeable rise in the LCOE. On the other hand, when CAPEX is reduced by 5%, 10%, 15%, or 20%, the LCOE correspondingly decreases.

The trend demonstrates a strong linear relationship between CAPEX and LCOE. Moreover, the graph shows that the total range of LCOE values becomes much larger when CAPEX is adjusted under higher OPEX conditions. In some scenarios, especially those with the highest OPEX variation, the LCOE increases significantly—from approximately 8 USD cents to nearly 13 USD cents per kilowatt-hour. This shows how sensitive the LCOE is to investment cost, particularly when other cost components are also elevated.

These results emphasize that CAPEX is a major factor influencing the economic outcome of the system. Even relatively small adjustments in capital cost can cause considerable changes in the final LCOE, making it essential to carefully plan and manage investment costs during system design and development.

The impact of OPEX variation on LCOE is shown in Fig. 16. The figure illustrates that as the percentage of OPEX increases, the resulting LCOE also rises accordingly. Similar to the pattern observed in the CAPEX variation analysis, this result also shows that when the OPEX percentage is calculated based on the highest adjusted CAPEX value, the difference in LCOE becomes more significant. For example, when OPEX is varied from 2% to 6% of the highest CAPEX, the change in LCOE can reach up to 3 USD cents. This trend is consistent across all depths, with the lowest LCOE values achieved at a depth of 600 m.

From both Fig. 15 and Fig. 16, it is evident that CAPEX and OPEX are closely interconnected in influencing the LCOE. While CAPEX directly affects the initial investment cost, OPEX contributes to long-term operational expenses. When both parameters are increased simultaneously, the LCOE can rise significantly, as seen in the scenarios with the highest CAPEX and OPEX combinations. Therefore, the integration of CAPEX and OPEX must be considered carefully in the planning and design stages of OTEC systems, as their combined effect plays a crucial role in determining the overall economic feasibility.

5. Conclusion

This study applies both technical and economic approaches to evaluate the influence of deep seawater intake depth on the performance of Ocean Thermal Energy Conversion (OTEC) systems. The analysis considered surface seawater at a depth of 20 m and cold seawater intake depths of 350, 400, 500, 600, and 700 m. The technical evaluation focused on system efficiency and key design parameters, while the economic assessment was conducted using the Levelized Cost of Energy (LCOE). To ensure the reliability of the modeling framework, the thermodynamic model applied in this study was validated against experimental results reported in the literature, showing good agreement between the predicted and experimental performance values. This validation confirms that the adopted approach is sufficiently reliable for assessing the technical and economic performance of OTEC systems under different seawater intake depths.

The results show that increasing the deep seawater intake depth increases the temperature difference between surface and deep seawater, which improves the thermodynamic performance of the OTEC system. The most significant improvement occurs between 350 m and 400 m, where the reduction in deep seawater temperature substantially enlarges the thermal gradient. Beyond this range, the temperature decrease becomes more gradual, resulting in smaller incremental performance gains. Among the evaluated configurations, the system operating with a 700 m cold seawater intake achieved the highest thermal efficiency of 3.75% and produced the greatest Annual Energy Production (AEP), reaching 871,068.6 MWh.

The larger thermal gradient also reduces the required mass flow rate of both seawater and working fluid, since the heat exchangers can transfer the required thermal energy with a smaller fluid volume. Consequently, deeper intake depths lead to smaller heat exchanger surface areas and slightly reduced seawater pipe diameters. Although the reduction in pipe diameter remains relatively small across the investigated depths, the decrease in mass flow rate contributes to lower infrastructure requirements. However, deeper intake depths increase the pumping head of the cold seawater pump, which slightly raises the pumping power demand.

From an economic perspective, the reduction in heat exchanger surface area plays a key role in lowering capital expenditures (CAPEX), as evaporators and condensers represent major cost components in the

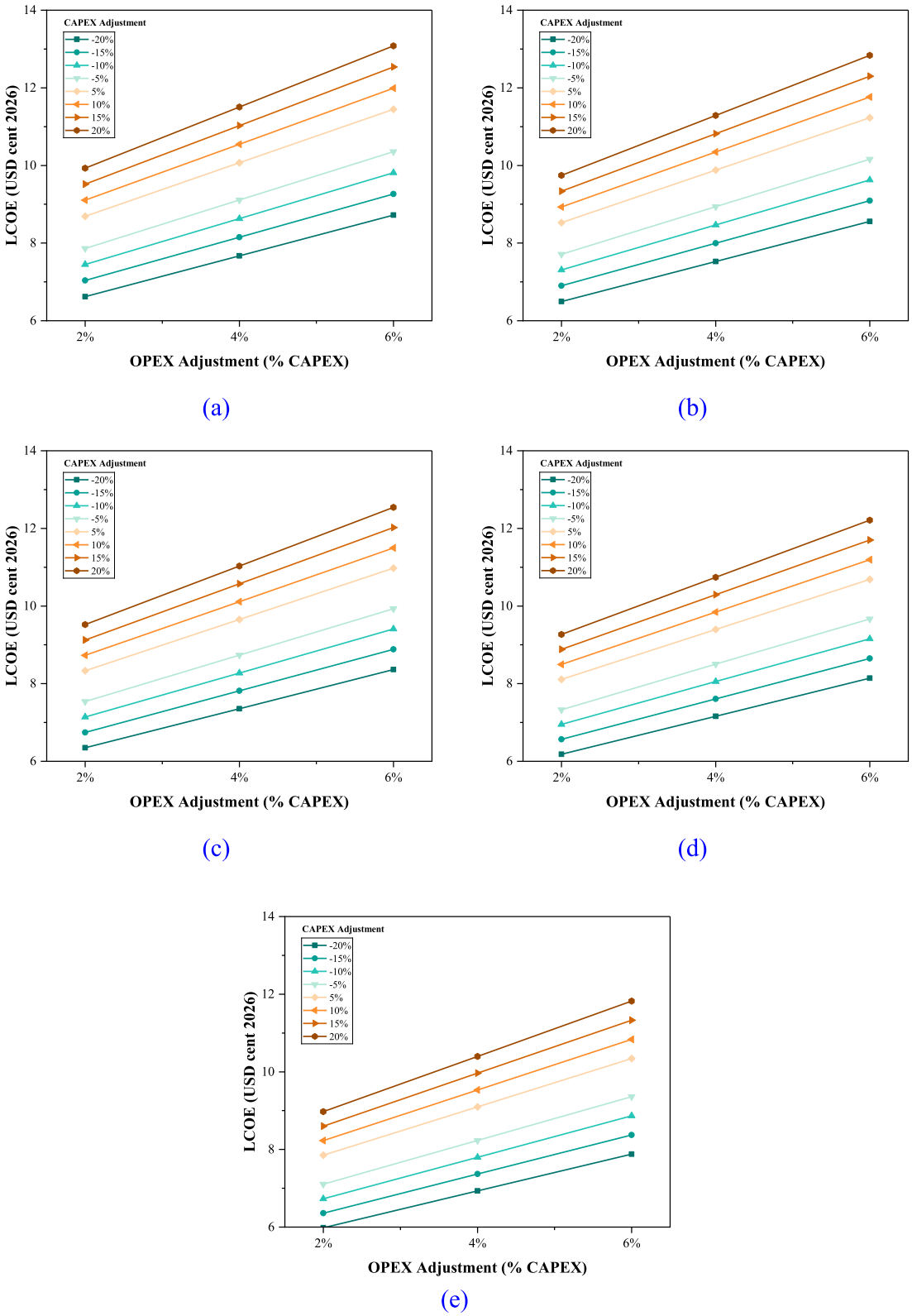

Fig. 16. Effect of OPEX Adjustment on LCOE at Different Depths: (a) 350 m; (b) 400 m; (c) 500; (d) 600; and (e) 600 m.

OTEC system. Although certain components such as deep seawater pipes and pumping systems increase slightly with depth, the overall CAPEX decreases because the cost reduction in thermal components outweighs the additional structural costs. As a result, the lowest LCOE of 8.31 USD cents/kWh was obtained at the 700 m intake depth.

The sensitivity analysis further demonstrates that the LCOE is strongly affected by variations in CAPEX and OPEX. In particular, the economic performance of the system is most sensitive to major capital components such as the platform, installation, and heat exchangers. In several scenarios, simultaneous increases in CAPEX and OPEX can raise

the LCOE from approximately 8 USD cents/kWh to nearly 13 USD cents/kWh. These results highlight the importance of carefully integrating both investment and operational cost considerations during the early design stage to ensure a realistic assessment of OTEC project feasibility.

Overall, the results indicate that OTEC systems utilizing deeper cold seawater intake can achieve improved thermodynamic performance and lower electricity costs. Such systems have strong potential for tropical coastal regions and island communities where a stable and continuous renewable energy supply is required. In particular, OTEC could contribute to reducing dependence on diesel-based electricity generation in remote island regions and improving long-term energy security.

Despite these promising results, several limitations remain. The analysis relies on site-specific temperature profiles derived from HYCOM data and does not explicitly consider the potential environmental impacts associated with large-scale cold seawater extraction. Future studies should therefore focus on validating ocean temperature data through direct field measurements, assessing the ecological impacts of sustained cold-water intake operations, and conducting more comprehensive evaluations of exergy loss distribution and operational stability under varying intake depths.

Declaration of Competing Interest

The authors declare that they have no known competing financial interests or personal relationships that could have appeared to influence the work reported in this paper.

Acknowledgement

The present study was supported by PT. PLN Indonesia under grand contract number 1928.Pj/DAN.01.02/F01040100/2023 or 0309.1.00/IT2.IV.3/KS.00.03/2023.

Data availability

Data will be made available on request.

References

Achkienasi, A., Silva, R., Mendoza, E., Luna, L.D., 2024. Choosing the most suitable working fluid for a CTEC. Energies 17. https://doi.org/10.3390/en17092181.

Adiputra, R., Rasgianti, Nugraha, A.D., Puryantini, N., Salamena, G.G., Prabowo, A.R., 2025. Comprehensive assessment of working fluid selection for ocean thermal energy conversion. Results Eng. 28, 108086. https://doi.org/10.1016/j.rineng.2025.108086.

Adiputra, R., Utsunomiya, T., 2021. Linear vs non-linear analysis on self-induced vibration of OTEC cold water pipe due to internal flow. Appl. Ocean Res. 110, 102610. https://doi.org/10.1016/j.apor.2021.102610.

Al Kautsar, H.A., Adiputra, R., Kusharjanta, B., Prabowo, A.R., Puryantini, N., Salamena, G.G., Riyalda, B.F., Melnyk, O., Jurkovič, M., 2025. Flexural capacity evaluation of OTEC piping system: finite element analysis and governing formula. J. Mar. Sci. Appl. https://doi.org/10.1007/s11804-025-00675-8.

Aresti, L., Christodoulides, P., Michailides, C., Onoufriou, T., 2023. Reviewing the energy, environment, and economy prospects of Ocean Thermal Energy Conversion (OTEC) systems. Sustain. Energy Technol. Assess. 60, 103459. https://doi.org/10.1016/j.seta.2023.103459.

Aresti, L., Onoufriou, T., Michailides, C., Christodoulides, P., 2025. Ocean thermal energy conversion systems: The heat losses effect of the cold-water pipe. Case Stud. Therm. Eng. 74, 106746. https://doi.org/10.1016/j.csite.2025.106746.

Avery, W.H., Wu, C., 1994. Renewable energy from the ocean: a guide to OTEC. Oxford University Press.

Azmi, A.A., Yasunaga, T., Fontaine, K., Morisaki, T., Nakaoka, T., Thirugnana, S.T., Jaafar, A.B., Ikegami, Y., 2024. Basic design optimization of power and desalinated water for hybrid cycle ocean thermal energy conversion system integrated with desalination plant. J. Mar. Sci. Technol. 29, 333–352. https://doi.org/10.1007/s00773-024-00988-3.

Bernardoni, C., Binotti, M., Giostri, A., 2019. Techno-economic analysis of closed OTEC cycles for power generation. Renew. Energy 132, 1018–1033. https://doi.org/10.1016/j.renene.2018.08.007.

Bosch, J., Staffell, I., Hawkes, A.D., 2019. Global levelised cost of electricity from offshore wind. Energy 189, 116357. https://doi.org/10.1016/j.energy.2019.116357.

Chung, Y.C., Wu, C.I., 2024b. Efficiency enhancement in ocean thermal energy conversion: a comparative study of heat exchanger designs for Bi2Te3-based thermoelectric generators. Materials 17. https://doi.org/10.3390/ma17030714.

Chung, Y.C., Wu, C.I., 2024a. Enhancing ocean thermal energy conversion performance: optimized thermoelectric generator-integrated heat exchangers with longitudinal vortex generators. Energies 17. https://doi.org/10.3390/en17020526.

Ciappi, L., Socci, L., Calabrese, M., Di Francesco, C., Savelli, F., Manfrida, G., Rocchetti, A., Talluri, L., Fiaschi, D., 2024. Exploiting the Ocean Thermal Energy Conversion (OTEC) technology for green hydrogen production and storage: exergo-economic analysis. Int. J. Hydrog. Energy 92, 1448–1462. https://doi.org/10.1016/j.ijhydene.2024.10.290.

Cong, W., Zhao, Y., Du, B., 2025. A components' layout optimization design method considering mass and thermal characteristics. Eng. Optim. 1–27. https://doi.org/10.1080/0305215X.2024.2433078.

Faizatama, A.M., Firdaus, N., Adiputra, R., Prabowo, A.R., Ghanbari-Ghazijahani, T., Fazeres-Ferradosa, T., Melnyk, O., Salamena, G.G., 2025. Hydrodynamic impact of cold-water pipes and mooring systems on KVLCC2 for floating OTEC platforms. Ocean Eng. 341, 122491. https://doi.org/10.1016/j.oceaneng.2025.122491.

Firmansyah, A.I., Mukhtasor, Satrio, D., Rahmawati, S., Ikhwani, H., Pratikto, W.A., 2024. A study of the temperature distribution in the OTEC cold water pipe using a heat and mass transfer approach. IOP Conf. Ser. Earth Environ. Sci. 1372. https://doi.org/10.1088/1755-1315/1372/1/012018.

Fontaine, K., Yasunaga, T., Ikegami, Y., 2025. Ocean thermal energy conversion net power maximization for the optimization of plate heat exchanger geometry. Int. J. Thermofluids 26, 101115. https://doi.org/10.1016/j.ijft.2025.101115.

G. Petterson, M., Ju Kim, H., 2020. Can Ocean Thermal Energy Conversion and Seawater Utilisation Assist Small Island Developing States? A Case Study of Kiribati, Pacific Islands Region. Ocean Therm. Energy Convers. - Present. Prog. https://doi.org/10.5772/intechopen.91945.

Habib, M.I., Adiputra, R., Prabowo, A.R., Erwandi, E., Muhayat, N., Yasunaga, T., Ehlers, S., Braun, M., 2023. Internal flow effects in OTEC cold water pipe: Finite element modelling in frequency and time domain approaches. Ocean Eng. 288, 116056. https://doi.org/10.1016/j.oceaneng.2023.116056.

Hisamatsu, R., Utsunomiya, T., 2024. Floating OTEC Plant—A Design and Coupled Dynamics. pp. 611–629. https://doi.org/10.1007/978-981-97-0495-8_36.

IEA-OES, 2024. Ocean Thermal Energy Conversion (OTEC) Economics: Updates and Strategies.

Kim, A.S., Kim, H., Lee, H., Cha, S., 2016. Dual-use open cycle ocean thermal energy conversion (OC-OTEC) using multiple condensers for adjustable power generation and seawater desalination. Renew. Energy 85, 344–358. https://doi.org/10.1016/j.renene.2015.06.014.

Kim, H.J., Lee, H.S., Jung, Y.K., Cha, S.W., Moon, D.S., 2014. Design, fabrication, and performance test of R32-OTEC pilot plant. ASME 2014 8th Int. Conf. Energy Sustain. ES 2014 Collocated ASME 2014 12th Int. Conf. Fuel Cell Sci. Eng. Technol. 1, 2014–2017. https://doi.org/10.1115/ES2014-6422.

Langer, J., Blok, K., 2023. The global techno-economic potential of floating, closed-cycle ocean thermal energy conversion. J. Ocean Eng. Mar. Energy. https://doi.org/10.1007/s40722-023-00301-1.

Langer, J., Blok, K., 2024. The global techno-economic potential of floating, closed-cycle ocean thermal energy conversion. J. Ocean Eng. Mar. Energy 10, 85–103. https://doi.org/10.1007/s40722-023-00301-1.

Langer, J., Infante Ferreira, C., Quist, J., 2022. Is bigger always better? Designing economically feasible ocean thermal energy conversion systems using spatiotemporal resource data. Appl. Energy 309, 118414. https://doi.org/10.1016/j.apenergy.2021.118414.

Liu, T., Hirose, N., Yamada, H., Ikegami, Y., 2020. Estimation of ocean thermal energy potential in the Aguni Basin. Appl. Ocean Res. 101. https://doi.org/10.1016/j.apor.2020.102185.

Lu, H., Fan, C., Li, D., Chen, Y., Yao, F., 2025. Economic and exergy assessments for ocean thermal energy conversion using environment-friendly fluids. Processes 13, 1–18. https://doi.org/10.3390/pr13092780.

Lu, B., Liu, Y., Zhai, X., Zhang, L., Chen, Y., 2024. Design and experimental study of 50 kW ocean thermal energy conversion test platform based on organic rankine cycle. J. Mar. Sci. Eng. 12. https://doi.org/10.3390/jmse12030463.

Makai Ocean Engineering, 2020. Ocean Thermal Energy Conversion (OTEC) [WWW Document]. URL ⟨https://www.makai.com/renewable-energy/otec/⟩ (accessed 10.26.23).

Mao, L., Wei, C., Zeng, S., Cai, M., 2023. Heat transfer mechanism of cold-water pipe in ocean thermal energy conversion system. Energy 269, 126857. https://doi.org/10.1016/j.energy.2023.126857.

Martel, L., Smith, P., Rizea, S., Van Ryzin, J., Morgan, C., Noland, G., Pavlosky, R., Thomas, M., 2012. Ocean Thermal Energy Conversion Life Cycle Cost Assessment. Final Technical Report 161.

Mukhtasor, Firmansyah, A.I., Satrio, D., Rahmawati, S., Shadiq, R., Yaakob, O., 2024. On assessing a potential reuse of the indonesian post-operation offshore oil/gas pipelines as a cold-water pipE for an Ocean Thermal Energy Conversion (Otec) System: A Thermal and Fluid Dynamic Perspective. J. Adv. Res. Fluid Mech. Therm. Sci. 123, 53–68. https://doi.org/10.37934/arfmts.123.1.5368.

Nihous, G.C., 2007. A preliminary assessment of ocean thermal energy conversion resources. J. Energy Resour. Technol. 129, 10–17. https://doi.org/10.1115/1.2424965.

Oko, C.O.C., Obeneme, W.B., 2018. Thermo-economic analysis of an ocean thermal power plant for a Nigerian coastal region. Int. J. Ambient Energy 39, 562–572. https://doi.org/10.1080/01430750.2017.1318789.

Prasad, R.D., Ali, M., Ahmed, M.R., 2025. Experimental evaluation of the power output and efficiency of a small solar-boosted OTEC power plant. Energies 18. https://doi.org/10.3390/en18010127.

Puryantini, N., Satrio, D., Adiputra, R., Silvianita, 2026. The influence of ocean thermal energy conversion system efficiency on net power output. E3S Web Conf. 687, 01011. https://doi.org/10.1051/e3sconf/202668701011.

Rami, Y., Allouhi, A., 2024. 3 E (Energy, Exergy and Economic) multi-objective optimization of a novel solar-assisted ocean thermal energy conversion system for integrated electricity and cooling production. Energy Convers. Manag 321, 119006. https://doi.org/10.1016/j.enconman.2024.119006.

Rasgianti, Adiputra, R., Nugraha, A.D., Firdaus, N., Sitanggang, R.B., Puryantini, N., Yasunaga, T., 2024a. Design optimization of stiffening system for ocean thermal energy conversion (OTEC) cold water pipe (CWP). Results Eng. 23, 102863. https://doi.org/10.1016/j.rineng.2024.102863.

Rasgianti, Adiputra, R., Sitanggang, R.B., Puryantini, N., Firdaus, N., 2024c. Ocean Thermal Energy Conversions (OTEC) Working Fluid Comparison Based on the Numerical and Analytical Analysis, in: 2024. International Conference on Technology and Policy in Energy and Electric Power (ICTPEP). IEEE, pp. 222–227. https://doi.org/10.1109/ICT-PEP63827.2024.10733395.

Rasgianti, Adiputra, Nugraha, R., Sitanggang, A.D., Pandoe, R.B., Aprijanto, W.W., Yasunaga, T., Santosa, M.A., 2024b. System parameters sensitivity analysis of ocean thermal energy conversion. Emerg. Sci. J. 8, 428–448. https://doi.org/10.28991/ESJ-2024-08-02-04.

Rashid, A., Nakib, T.H., Shahriar, T., Habib, M.A., Hasanuzzaman, M., 2024. Energy and economic analysis of an ocean thermal energy conversion plant for Bangladesh: a case study. Ocean Eng. 293, 116625. https://doi.org/10.1016/j.oceaneng.2023.116625.

Saadha, A., Ishihara, K.N., Ogawa, T., Basu, S., Okumura, H., 2025. Techno-economic analysis of combined onshore ocean thermal energy conversion technology and seawater air conditioning in small island developing states. Sustainability 17, 4724. https://doi.org/10.3390/su17104724.

Shi, W., Sun, Y., Pan, L., Song, L., Wei, X., 2023. Objective functions and performance optimization of ocean thermal energy conversion (OTEC) with CO2-based binary zeotropic mixture power cycle. J. Mar. Sci. Eng. 11. https://doi.org/10.3390/jmse11010140.

Straatman, P.J.T., van Sark, W.G.J.H.M., 2008. A new hybrid ocean thermal energy conversion-Offshore solar pond (OTEC-OSP) design: a cost optimization approach. Sol. Energy 82, 520–527. https://doi.org/10.1016/j.solener.2007.12.002.

Tian, M., Yu, Y., Hou, Y., Chen, Y., Zhang, L., Liu, Y., 2024. Optimization of ocean thermal energy conversion based on pressure energy recovery of ammonia water working medium. Front. Energy Res. 12, 1–16. https://doi.org/10.3389/fenrg.2024.1472980.

Tobal-cupul, J.G., Garduño-ruiz, E.P., Gorr-pozzi, E., Olmedo-gonz, J., Diane, E., Navarro-moreno, D.D., Emmanuel, J., Garc, F., Wang, M., Zamora-castillo, S., Rodr, Y., Rivera, G., Garc, A., Zertuche-gonz, A., 2022. An assessment of the financial feasibility of an OTEC Ecopark: a case study at Cozumel Island. Sustainability.

Upshaw, C.R., 2012. Thermodynamic and economic feasibility analysis of a 20 MW Ocean Thermal Energy Conversion (OTEC). Power 171.

Visser, E., Held, A., 2014. Methodologies for estimating Levelised Cost of Electricity (LCOE) Implementing the best practice LCoE methodology of the guidance Methodologies for estimating Levelised Cost of Electricity (LCOE). Ecofys 35.

Wang, Y., Liu, Y., Zhang, Q., 2024. Auxiliary heat system design and Off-design performance optimization of OTEC radial inflow turbine. Energies 17. https://doi.org/10.3390/en17112767.

Yang, M.H., Yeh, R.H., 2014. Analysis of optimization in an OTEC plant using organic Rankine cycle. Renew. Energy 68, 25–34. https://doi.org/10.1016/j.renene.2014.01.029.

Zhang, Y., Li, Y., Tian, Z., Yang, C., Peng, H., Kan, A., Gao, W., 2025. Thermodynamic performance prediction and optimization of a 1 kW ocean thermal energy cogeneration system based on artificial neural network. Energy 314, 134264. https://doi.org/10.1016/j.energy.2024.134264.

Zhang, K., Lv, X., Weng, Y., 2024. Effect of working fluid on the ORC cycle performance of the ocean thermal energy conversion system. J. Phys. Conf. Ser. 2707. https://doi.org/10.1088/1742-6596/2707/1/012102.

Zhou, Y., Gao, W., Zhang, Y., Tian, Z., Tian, Y., Yang, C., 2025. Effect of working fluid charging amount on system performance in an ocean thermal energy conversion system. Appl. Therm. Eng. 258, 124753. https://doi.org/10.1016/j.applthermaleng.2024.124753.